SPIN-05/15
ITP-UU-05/19

Counting a black hole in Lorentzian product triangulations

B. Dittrich [a] and *R. Loll* [b]

[a] Max-Planck-Institute for Gravitational Physics,
Am Mühlenberg 1, D-14476 Golm, Germany.
email: dittrich@aei-potsdam.mpg.de

[b] Institute for Theoretical Physics, Utrecht University,
Leuvenlaan 4, NL-3584 CE Utrecht, The Netherlands.
email: r.loll@phys.uu.nl

Abstract

We take a step toward a nonperturbative gravitational path integral for black-hole geometries by deriving an expression for the expansion rate of null geodesic congruences in the approach of causal dynamical triangulations. We propose to use the integrated expansion rate in building a quantum horizon finder in the sum over spacetime geometries. It takes the form of a counting formula for various types of discrete building blocks which differ in how they focus and defocus light rays. In the course of the derivation, we introduce the concept of a Lorentzian dynamical triangulation of product type, whose applicability goes beyond that of describing black-hole configurations.

1. Introduction

Very encouraging progress has been made recently in constructing *spacetime* dynamically from a nonperturbative gravitational path integral, by studying the continuum limit of causal dynamical triangulations [1, 2, 3, 4]. The quantum geometries generated in this way exhibit semiclassical properties at sufficiently large scales: they are four-dimensional [5, 6] and the large-scale dynamics of their spatial volume is described by an effective cosmological minisuperspace action [7]. Their short-distance behaviour is highly nonclassical, including a smooth dynamical reduction of the spectral dimension from four to two [8] and evidence of fractality [6].

A question frequently asked of this and other approaches to quantum gravity is what they have to say about the quantum dynamics of black holes and, more specifically, whether the black-hole entropy "comes out right". What is usually meant by this is whether the theory can reproduce the Bekenstein-Hawking formula $S = A/4$ which relates the entropy S of a black hole to its area A in Planck units, and preferably at the same time provide a microscopic explanation of the presence of black-hole entropy in terms of fundamental excitations of geometry (see [9, 10, 11] for recent reviews). Although often portrayed as a touchstone for quantum gravity, it should be kept in mind that the entropy formula and other thermodynamic relations satisfied by black holes are semiclassical. Whether or not they have a fundamental role to play in a genuinely nonperturbative formulation of the theory remains to be seen.

This naturally raises the question whether the approach of causal dynamical triangulations, which we believe is a strong candidate for a nonperturbative theory of four-dimensional quantum gravity, can provide new insights into the quantum properties of black holes. Apart from having already reproduced certain classical aspects of general relativity from first principles, the fact that the causal, Lorentzian structure of spacetime geometry plays a central role and that a well-defined Wick rotation is available at the regularized level seem to make this formulation particularly suited for addressing issues to do with black holes. However, putting this into practice turns out to be a challenging proposition. Not only are there technical obstacles to be overcome, but one also has to decide what precise quantity should be calculated *if* one were given a well-defined method for performing nonperturbative sums over geometries, such as causal dynamical triangulations, a question that has hardly begun to be addressed.

The main choices to be made when setting up the path integral are that of an ensemble of geometries to be summed over, and of boundary conditions for the geometries. Since numerical evaluations of the path integral must necessarily take place in a finite spacetime volume, boundary conditions will have to be provided not only on some initial and final spatial slice, but also on a (timelike) boundary

at large radius, and potentially also on a hypersurface at small radius to avoid any central singularity.[1] We will for the moment set aside the question of how the boundary conditions should be chosen, and how many black holes one can expect to generate dynamically as a function of the boundary data. Instead we will focus on an issue that will be relevant regardless of the geometric ensemble and boundary conditions chosen, namely, which observable in the quantum theory can give us information about the presence or otherwise of a black-hole configuration. In a fully nonperturbative formulation, this is a difficult task because of the absence of a classical background structure. In the nonperturbative path integral, all possible geometries are superposed, not just those which represent fluctuations around a given classical background geometry. Semiclassical geometry emerges only in the continuum limit and at sufficiently large scales [7, 6]. The problem is then how and where in the dynamically generated quantum geometry one should look for evidence of a black hole, say, an apparent horizon.

To simplify matters slightly, we will consider geometries with at most a single black hole, and which moreover have (an approximate) spherical symmetry. To translate these conditions to the setting of causal dynamical triangulations, a useful concept is that of *triangulations of product type*. These are roughly speaking simplicial analogues of fibred spaces, with a triangulated base space and triangulated fibres. The inspiration for such structures comes in part from Lorentzian semi-random lattices [13], which in turn were motivated by causal triangulated models of quantum gravity in lower dimensions [1, 3].[2]

In the context of a nonperturbative description of four-dimensional black holes, we propose to use triangulations of product type whose base space is a simplicial version of the r-t-plane, with fibres representing the two angular directions. For simplicity, it seems a good strategy not to include completely general geometries (triangulations) of this type in the path integral initially, but only a subset which satisfies certain homogeneity requirements along the angular directions, implementing an approximate spherical symmetry at a coarse-grained scale. The fact that an exact continuous rotation symmetry cannot even in principle be realized by the simplicial structures we are working with is not at all a drawback, but simply implies that the path integral will necessarily include fluctuations which violate spherical symmetry, especially at short distances. This is desirable from the point of view of the quantum theory, because it is likely

[1] A detailed discussion of the inclusion of boundary terms in causal dynamical triangulations can be found in [12].

[2] The presence of a Möbius inversion formula for such semi-random lattices, relating their partition function to that of a statistical model of geometric objects of one dimension less (see also [14]), may help to solve these models analytically. In the context of three-dimensional quantum gravity in terms of causal dynamical triangulations, this possibility is currently being explored [15]. A related quantum-cosmological model which introduces more "order" in three-dimensional random triangulations is described in [16].

to make the model closer to the full theory than gravitational models where an exact symmetry reduction is performed *before* the quantization (see [17] for an analogous reasoning in canonical quantum gravity).

In the present work, we will not attempt to define and evaluate a nonperturbative path integral for black holes, but pursue a more modest goal, namely, to formulate a geometric observable for dynamical triangulations to help to determine the "presence" (in the sense of expectation values) of a black hole in the quantum theory. The observable is a simplicial version of the integrated expansion rate for light rays, whose vanishing in the classical continuum theory is an indicator of the presence of an apparent horizon. We derive an analogous quantity for causal dynamical triangulations which has a particularly simple form, and which we hope can be used to construct an efficient "horizon finder" in Monte Carlo simulations of the quantum theory. It depends only on the numbers of simplicial building blocks of various types and orientations occurring in a given fibre of the product triangulation, but *not* on how these building blocks are glued together locally. In this sense, the presence of an apparent horizon can be established simply by counting.[3]

The rest of the paper is structured as follows. In Sec. 2 we introduce the general concept of a Lorentzian triangulation of product type, before specializing to the case of a two-dimensional base space. For product triangulations in 2+1 and 2+2 dimensions, we classify all simplices occurring in the fibres according to their orientation and derive some topological relations among them. Sec. 3 is devoted to a discussion of extrinsic curvatures and expansion rates. We start by recalling the classical notion of a trapped surface and compute the light expansion rates on a surface of codimension 2 from the extrinsic curvatures and other geometric data. We then repeat the calculation for piecewise flat manifolds, by employing a careful limiting process at the "kinks" of the triangulation.[4] This sets the stage for computing the integrated expansion rates for causal dynamical triangulations. We derive the "counting formulas", our main result, in both 2+1 and 2+2 dimensions, and also give a qualitative interpretation in terms of the focussing and defocussing of light rays by particular types of simplices. In Sec. 4, we construct an explicit example of a triangulated black hole in the formalism of Lorentzian product triangulations, and Sec. 5 contains a summary and outlook. The appendix deals with the definition of affine coordinates, which are used in some of our derivations. – Part of the work presented here is contained in the diploma thesis of one of the authors [19].

[3]To avoid any misunderstandings, let us emphasize that this counting has nothing to do with a counting of microstates to obtain an entropy for a black hole.

[4]A related treatment in the context of classical Regge calculus has appeared previously in [18].

2. Lorentzian triangulations of product type

A triangulated manifold $\mathcal{T}$ of product type is a particular case of a simplicial manifold. Topologically speaking, it is a cartesian product $\mathcal{T} = B \times F$ of a b-dimensional base space B with an f-dimensional fibre space F. A simplicial realization of this structure consists of a simplicial base manifold B, where to each k-dimensional simplex, $0 \leq k \leq b$, (k-simplex for short) σ of B we associate a so-called *σ-tower*, which is a particular triangulation of $\sigma \times F$, whose top-dimensional simplices are of dimension $k+f$. We will only consider triangulations $\mathcal{T}$ with a finite number of d-simplices. For $k=b$, the dimension of the simplices in the σ-towers is maximal, and coincides with the dimension $d=b+f$ of $\mathcal{T}$. The triangulations of these towers as well as the number of d-simplices they contain will in general depend on the b-dimensional base simplex σ. In order that the σ-towers fit together in a simplicial manifold, neighbouring towers have to satisfy matching conditions along their common $(d-1)$-dimensional boundaries, which themselves are σ-towers over the $(b-1)$-dimensional simplices of the base manifold B. The triangulations of the d-dimensional towers induce triangulations on all lower-dimensional σ-towers, that is, on the vertex towers, the edge towers, etc. By definition, each vertex of a product triangulation lies in precisely one vertex tower.

The focus of our interest will be on Lorentzian triangulations of product type, and our main applications will have a two-dimensional base triangulation. Note that the simplicial manifolds one considers in the approach of causal dynamical triangulations can be thought of as a special class of triangulations of product type, with base space B the one-dimensional proper-time direction, and fibre F a spatial hypermanifold of constant time. The simplicial realization of B is simply a one-dimensional chain of time-like edges, all of equal length. For d-dimensional simplicial spacetimes, the spatial slices of constant integer time t are the $(d-1)$-dimensional vertex towers over the (zero-dimensional) vertices of B, and the minimal spacetime "sandwiches" between times t and $t+1$ are the edge towers over B. Each vertex of the spacetime triangulation lies in the vertex tower of exactly one vertex in B and thus inherits an integer time coordinate.

The simplest non-trivial case of a causal triangulation is in dimension two, an example of which is depicted in Fig. 1. The vertex towers are one-dimensional chains of spatial edges or links, and the edge towers are linear sequences of two-dimensional triangles pointing up or down. In a useful notation that generalizes to more complicated examples, we denote an up-triangle by $[2, 1]$ ("two vertices in the tower above the base vertex at time t, one vertex in the tower above the base vertex at $t+1$"), and a down-triangle by $[1, 2]$ (the converse). Each strip is uniquely characterized by a sequence of such number pairs. Analogously, the d-simplices in a minimal spacetime sandwich of a d-dimensional causal triangulation $\mathcal{T}$ can

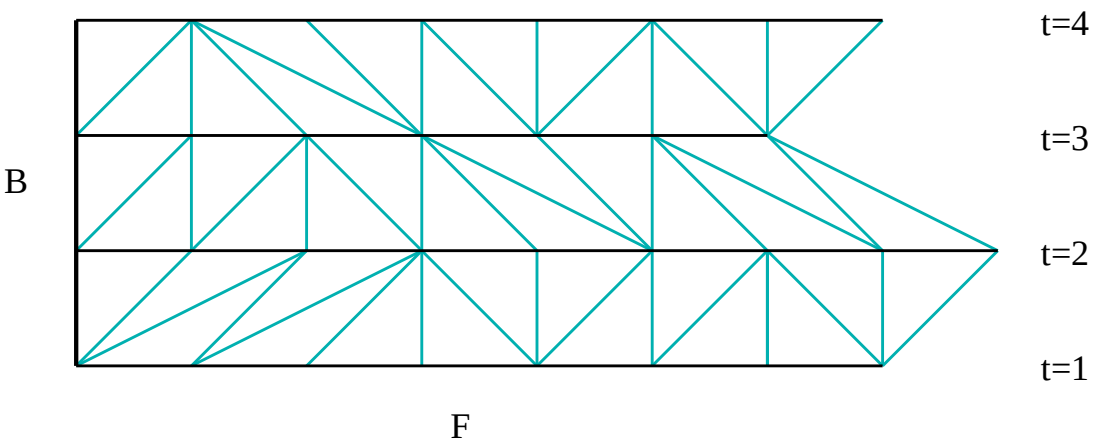

Figure 1: Example of a two-dimensional Lorentzian triangulation $\mathcal{T}$ whose base space B is the one-dimensional triangulation consisting of three timelike edges. Note that in our graphical representation lengths are *not* represented isometrically, in fact, this is impossible because of the intrinsic curvature carried by $\mathcal{T}$. There is only one type of triangular building block which appears with either up- or down-orientation. Consequently, all spacelike edges (horizontal) and all timelike edges (interpolating between adjacent slices of constant integer time) have identical length, although the latter fact is not rendered faithfully in the figure.

be characterized by a pair $[i_1, i_2]$, $i_k \in \{1, \ldots, d\}$, where i_1 counts the number of vertices at time t and i_2 those at time $t+1$ [4]. Since a d-simplex has $d+1$ vertices, there are d different ways how its vertices can be distributed over the two constant-time slices, leading to configurations of type $[d, 1]$, $[d-1, 2]$, ..., $[1, d]$.

The product triangulations we will consider are Lorentzian, that is, they are assembled from flat d-dimensional Minkowskian simplicial building blocks and have a product structure with respect to the time direction. We show in the appendix that in such manifolds the notion of a constant-time slice can be extended naturally to non-integer t. The resulting $(d-1)$-dimensional hypersurfaces are again piecewise flat, but the individual building blocks are not necessarily simplices (for example, the intersection pattern obtained by cutting through a three-dimensional Lorentzian triangulation is a simplicial manifold consisting of triangles and rectangles). These concepts can be extended straightforwardly to the case where the base manifold B is higher-dimensional. Because of the Lorentzian structure of the triangulation, one of the directions in B will be the time direction. For example, in the simplicial analogues of spherically symmetric models discussed below, $\dim(B) = 2$, with one time t and one radial direction r. Also in this case, there will be a well-defined notion of an f-dimensional fibre

F over an arbitrary non-integer base point (t, r). This fibre takes the form of a piecewise flat manifold, with generalized flat building blocks.

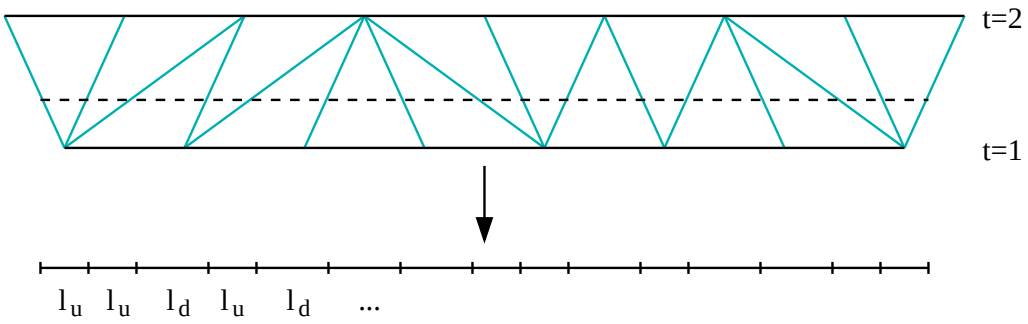

Figure 2: An edge tower $\sigma \times F$ of a two-dimensional Lorentzian triangulation can be represented by a one-dimensional graph consisting of long and short edges which corresponds to a cut through the tower at some time which does not coincide with $t = 1/2$. In the figure, the cut at $t < 1/2$ is indicated by the dashed line, the short edges have length l_u and the long ones l_d. Because of our planar representation, the horizontal distances in the interior of the strip are again not rendered faithfully.

An important and useful observation is the fact that the d-dimensional geometry of a σ-tower, where σ is a b-simplex in B, can be deduced entirely from the geometry of the fibre F over a single interior point of σ. A simple example is again given by a two-dimensional Lorentzian triangulation. The fibre of constant time s over some interior point s of a strip $[t, t{+}1]$, with t an integer, is a sequence of straight edges. In order to be able to distinguish the edges that come from cutting up- and down-triangles, we must choose $s \neq t{+}1/2$ (a similar exclusion of symmetric points applies also in more complicated examples). This will result in edges of two different lengths l_u and l_d, as depicted in Fig. 2, and it is obvious that we can reconstruct the entire strip (or σ-tower) from the knowledge of the sequence of the two types of edges occurring in the fibre over s. An alternative way of keeping track of the two different types of edge that can occur in the tower is to colour-code them (Fig. 3). Both procedures generalize to more complicated product manifolds, with each σ-tower represented uniquely by either a (generalized) f-dimensional triangulations or a special type of multicoloured graph (see the following sections for further examples, and the appendix for geometric details), and the matching conditions for σ-towers taken into account appropriately.

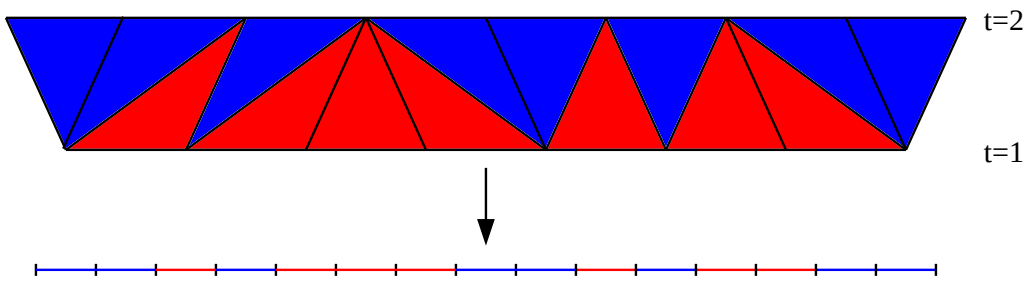

Figure 3: Alternatively, the same edge tower can be represented by a one-dimensional graph consisting of edges of two colours, which can be thought of as being induced from colouring the up- and down-triangles differently and considering a cut at midtime $t=1.5$.

2.1 Lorentzian product triangulation with two-dimensional base

In preparation for later sections, we will now describe the geometry of Lorentzian triangulations $\mathcal{T}$ with a two-dimensional base space, for $d=2+1$ and $d=2+2$. In both cases, the top-dimensional simplices of B are two-dimensional triangles, and $\mathcal{T}$ consists of triangle towers. By assumption, the base manifold is itself of the form of a (1+1)-dimensional Lorentzian product triangulation $B=B'\times F'$, of the type usually considered in two-dimensional causal dynamical triangulations [1] and depicted in Fig. 1 above. Its base B' is a one-dimensional triangulation consisting of timelike edges σ', with associated edge towers $\sigma'\times F'$ consisting of sequences of up- and down-triangles in the spatial direction. For our general discussion, it will not play a role whether the topology of these strips is spatially open or closed. Note that because of the physical interpretation of the triangulations as causal spacetime geometries, there is no symmetry between the time and spatial direction of B. Since the number of triangles in an edge tower $\sigma'\times F'$ is in general a function of time, B cannot be thought of as a product triangulation with the spatial direction as its base.

It follows that our simplicial manifolds have the form of "staggered" product triangulations, which can be thought of as fibrations over B or B'. Accordingly, their d-simplices can be characterized by how they fit into either of these product structures. The information concerning the fibration $\mathcal{T}=B'\times F'$ is simply the number pair $[i_1,i_2]$ which counts how many vertices of the simplex lie in either one of the two adjacent slices of constant time t, as described above. From this specification one can uniquely deduce the geometry of the d-simplex, i.e. which of its edges are spacelike and which are timelike, and compute all volumes and angles of the simplex and its subsimplices. Analogously, the orientation of a d-

simplex with respect to the fibration $\mathcal{T} = B \times F$ is specified by a triple of numbers $[j_1, j_2, j_3]$, which count how many of its $d+1$ vertices lie in each one of the three vertex towers contained in $\sigma \times F$.

2.2 The example of 2+1 dimensions

In order to train our geometric imagination, we start with the simpler case $d=3$ where the fibres F are one-dimensional. From the point of view of the time fibration $\mathcal{T} = B' \times F'$, the three-simplices or tetahedra come in three different time orientations, $[3,1]$, $[2,2]$ and $[1,3]$. From the point of view of the fibration $\mathcal{T} = B \times F$, there are three possibilities how a tetrahedron can appear in a tower above a given base triangle σ, which in an obvious notation are labelled by $[2,1,1]$, $[1,2,1]$ and $[1,1,2]$. Consequently, one can visualize the tower over σ as a prism with triangular base, which itself is of the form of a linear sequence of tetrahedra of these three types. Assigning three different colours to the differently oriented tetrahedra, we note that the geometry of the triangulated prism can be encoded in a one-dimensional graph made of edges of the three colours (Fig. 4), namely, the graph corresponding to the fibre over any interior point of σ. This is a three-dimensional analogue of the situation depicted in Fig. 3.

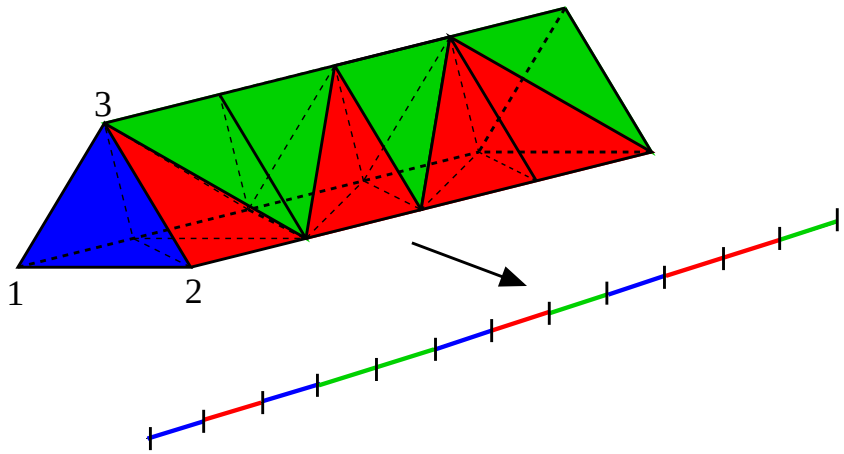

Figure 4: A triangle tower of a (2+1)-dimensional product triangulation can be represented by a one-dimensional graph consisting of edges of three colours, corresponding to a fibre over an interior point of the triangle. The three colours correspond to the different orientations with which a tetrahedron can appear in the prism. The figure depicts a sequence of tetrahedra $[2,1,1]$, $[1,2,1]$, $[2,1,1]$, $[1,1,2]$, etc., where the labels of the three vertex towers are as indicated.

In order to formulate the matching conditions between neighbouring triangle

simplex type \ in graph with colours	$i_1 i_2 i_3$	$i_1 i_2$	i_1
edge of colour i_1	$[2_{i_1}, 1_{i_2}, 1_{i_3}]$	$[2_{i_1}, 1_{i_2}, 0_{i_3}]$	$[2_{i_1}, 0_{i_2}, 0_{i_3}]$
vertex	$[1_{i_1}, 1_{i_2}, 1_{i_3}]$	$[1_{i_1}, 1_{i_2}, 0_{i_3}]$	$[1_{i_1}, 0_{i_2}, 0_{i_3}]$

Table 1: From this table, one reads off the unique building block $[j_{i_1}, j_{i_2}, j_{i_3}]$ in the triangle tower of a (2+1)-dimensional product triangulation corresponding to a simplex of a one-dimensional coloured graph (left column). The building block depends on the fibre type, as expressed by the number of colours occurring in the coloured graph to which the simplex belongs (top row). The three i_k are colour labels.

towers in this representation, one needs to translate the geometry of the edge tower common to the two triangle towers into a one-dimensional graph. One simply considers the fibre over an interior point of the edge in B in question. It is clear that this gives rise to a two-coloured graph, because it represents a cut through a two-dimensional triangulated strip. Denoting by σ_1 and σ_2 the two triangles in B adjacent to the edge, such a two-coloured graph is obtained by moving an interior point in one of the σ_i's toward the shared edge. In the process, one type of coloured edge disappears from the fibre above the point, because the corresponding type of tetrahedron shares only an edge with the common edge tower, and not a triangle. The matching condition can therefore be formulated as a condition on the linear graphs characterizing $\sigma_1 \times F$ and $\sigma_2 \times F$ with one colour each deleted.

We close this subsection with some further geometric observations, which are straightforward in a three-dimensional context, but generalize to the more difficult four-dimensional case. First, one may also associate a linear graph to a vertex tower, which can only ever consist of edges of a single colour. Second, to this graph and any other graph corresponding to a fibre over a point of σ the Euler relation

$$N_0 = N_1 + \rho \tag{1}$$

must apply, relating the number N_0 of vertices in the graph to the number N_1 of edges, irrespective of their colour. The variable ρ is either 0 or 1, depending on whether the graph topology is S^1 or $[0, 1]$. Table 1 lists which building block in the triangle tower corresponds to which element (vertex or coloured edge) of a one-dimensional coloured graph, depending on whether the graph comes from a fibre over an interior point of σ (and thus has three colours i_1, i_2, i_3), from a fibre over an edge (excluding the vertices) of σ (with two colours, e.g. i_1, i_2), or from a fibre over one of the three vertices (with a single colour) , e.g. i). For an

interior point of σ, relation (1) implies

$$N_{111} = N_{211} + N_{121} + N_{112} + \rho, \tag{2}$$

where the subscripts of the counting variables $N_{j_1 j_2 j_3}$ refer to the characterization of tetrahedra in the triangle tower according to the numbers $[j_1, j_2, j_3]$ of their vertices that lie in the vertex towers 1, 2 and 3. Subsimplices of a given tetrahedron inherit a triplet $[j_1, j_2, j_3]$ in an obvious way, with the three j_i adding up to the dimension of the subsimplex plus one. This accounts for the appearance of the counting number of triangles on the left-hand side of equation (2). Lastly, note that for the set of graphs associated with a given base triangle, edges of a particular colour occur with the same multiplicity in all graphs if the colour occurs in the graph at all. This translates into the relation

$$N_{211} = N_{210} = N_{201} = N_{200} \tag{3}$$

and permutations thereof. It follows that all numbers $N_{j_1 j_2 j_3}$ in one triangle tower are determined by N_{211}, N_{121} and N_{112}. Moreover, these three numbers are independent, since each type of tetrahedron can be inserted at any position of a triangular prism.

2.3 The example of 2+2 dimensions

In comparison with the previous subsection, we will use the same simplicial base space B, but increase the dimension of the fibre F from one to two. Let us call the spatial direction of the base space the "radial direction" (as will indeed be the case in later sections). The four possible types of four-simplices from the point of view of the time fibration are $[4, 1]$, $[3, 2]$, $[2, 3]$ and $[1, 4]$. These building blocks can still have different orientations within a given triangle tower. Without loss of generality, let us assume that the three vertices of the base triangle σ have coordinates (t_1, r_1), (t_1, r_2) and (t_2, r_3). For a $[4, 1]$-building block, say, there are now three possibilities how the four vertices in the vertex tower over the time t_1 (with respect to the fibration $B' \times F'$) can be distributed over the two vertex towers (t_1, r_1) and (t_1, r_2) (with respect to the fibration $B \times F$), labelled by $[3, 1, 1]$, $[1, 3, 1]$ and $[2, 2, 1]$. Similarly, a $[3, 2]$-building block can occur with two orientations, $[2, 1, 2]$ and $[1, 2, 2]$, but there is only a single way, $[1, 1, 3]$, to orient a $[2, 3]$-building block.

The question now arises of how the geometry of a triangle tower can be captured by looking at the two-dimensional B-fibres over (interior) points of its base triangle σ, which are cuts through $\mathcal{T}$ of constant time and radius. The top-dimensional building blocks of these surfaces are triangles (coming from $[3, 1, 1]$ and its permutations) and rectangles (from $[2, 2, 1]$ and its permutations). Like

simplex type	$B' \times F'$ type	fibre F'	fibre F	dual graph
$[3,1,1]$	$[4,1]$	tetrahedron	triangle rrr	3-val. vertex r
$[1,3,1]$	$[4,1]$	tetrahedron	triangle ggg	3-val. vertex g
$[1,1,3]$	$[2,3]$	prism	triangle bbb	3-val. vertex b
$[2,2,1]$	$[4,1]$	tetrahedron	rectangle grgr	4-val. vertex gr
$[2,1,2]$	$[3,2]$	prism	rectangle rbrb	4-val. vertex rb
$[1,2,2]$	$[3,2]$	prism	rectangle gbgb	4-val. vertex gb
$[2,1,1]$r	$[3,1]$	triangle r	edge r	edge r
$[1,2,1]$g	$[3,1]$	triangle g	edge g	edge g
$[1,1,2]$b	$[2,2]$	rectangle b	edge b	edge b
$[1,1,1]$	$[2,1]$	edge	vertex	polygon

Table 2: Four-simplices in the triangle tower over a base triangle with vertex coordinates (t_1, r_1), (t_1, r_2) and (t_2, r_3), how they appear in the product triangulation $B' \times F'$ with time base, and in the fibres F' and F, together with a dual representation of the latter. The three colours are indicated by r, g and b.

in previous examples, we can now colour-code subsets of edges in F that will always appear with a common length, independent of the base point in B of the fibre. Again they fall into three sets, which we will associate with the colours red, green and blue. The triangular building blocks in F are monochrome, while the rectangles are all bi-coloured, with opposite (and parallel) sides of identical colour. The fibre F therefore takes the form of a piecewise flat manifold with triangles and rectangles which are glued together along edges of identical colour.

Alternatively, it is sometimes convenient to use the graph dual to this (generalized) triangulation. Instead of triangles we then have dual monochrome trivalent vertices, and instead of the rectangles dual bi-coloured four-valent vertices, consisting of pairs of mutually crossing edges of different colour. Since the subgraphs of a single colour close on themselves, the dual graph has the form of a superposition of three trivalent monochrome planar graphs. Similar to what happened in the (2+1)-dimensional example, if the base point of the fibre is an interior point of an edge of σ, (dual) edges of one of the colours disappear, and if the base point coincides with a vertex of σ, there are only (dual) edges of a single colour left.

Summarizing our findings, we can say that the geometries of triangle, edge and vertex towers of a $(2+2)$-dimensional product triangulation are uniquely characterized by superpositions of three, two and a single monochrome trivalent

building block \ in dual graph	$i_1i_2i_3$	i_1i_2	i_1
3-val. vertex i_1	$[3_{i_1}, 1_{i_2}, 1_{i_3}]$	$[3_{i_1}, 1_{i_2}, 0_{i_3}]$	$[3_{i_1}, 0_{i_2}, 0_{i_3}]$
4-val. vertex i_1i_2	$[2_{i_1}, 2_{i_2}, 1_{i_3}]$	$[2_{i_1}, 2_{i_2}, 0_{i_3}]$	
edge i_1	$[2_{i_1}, 1_{i_2}, 1_{i_3}]$	$[2_{i_1}, 1_{i_2}, 0_{i_3}]$	$[2_{i_1}, 0_{i_2}, 0_{i_3}]$
polygon	$[1_{i_1}, 1_{i_2}, 1_{i_3}]$	$[1_{i_1}, 1_{i_2}, 0_{i_3}]$	$[1_{i_1}, 0_{i_2}, 0_{i_3}]$

Table 3: From this table, one reads off the unique building block $[j_{i_1}, j_{i_2}, j_{i_3}]$ in the triangle tower of a $(2+2)$-dimensional product triangulation corresponding to a building block of a dual planar coloured graph (left column). The building block $[j_{i_1}, j_{i_2}, j_{i_3}]$ depends on the fibre type, as expressed by the number of colours (three, two or one) occurring in the coloured graph to which the simplex belongs (top row). The three i_k are colour labels.

planar graph, respectively.[5] Table 2 summarizes the simplex types that can occur in a triangular tower, and how they appear with respect to the various fibrations.

With this characterization in hand, we can now apply the Euler relations for planar graphs,

$$\begin{aligned} &N_0^\star - N_1^\star + N_2^\star = \chi \\ &3N_0^{(3)\star} + 4N_0^{(4)\star} = 2N_1^\star, \end{aligned} \tag{4}$$

relating the numbers $N_d^\star$ of building blocks of dimension d contained in the dual graphs associated with a triangle tower. In (4), $N_0^\star = N_0^{(3)\star} + N_0^{(4)\star}$ is the sum of dual three- and four-valent vertices, $N_1^\star$ and $N_2^\star$ are the numbers of dual edges and faces, regardless of their colour, and χ is the Euler number of the fibre. Because there are different graphs associated with base points in the interior of the triangle σ, and its edges and vertices, (4) amounts to a total of 14 equations for the counting numbers $N_{j_1j_2j_3}$ for the various simplex types of a given triangle tower. They can be used to express $N_1^\star$ and $N_2^\star$ as functions of $N_0^{(3)\star}$ and $N_0^{(4)\star}$, say. Applying (4) to the graph representing the full triangle tower and making use of the "translation table", Table 3, we obtain

$$\begin{aligned} &N_{311}+N_{131}+N_{113}+N_{221}+N_{212}+N_{122}-N_{211}-N_{121}-N_{112}+N_{111} = \chi, \\ &3(N_{311}+N_{131}+N_{113})+4(N_{221}+N_{212}+N_{122}) = 2(N_{211}+N_{121}+N_{112}). \end{aligned} \tag{5}$$

[5]This picture is reminiscent of three-dimensional causal dynamical triangulations, where the three-dimensional 'sandwich' geometry of a discrete time step $\Delta t = 1$ can be represented by a dual graph which is a superposition of *two* monochrome trivalent planar graphs [20].

Furthermore, the numbers of three- and four-valent vertices of the same colour(s) are equal for each of the graphs in which they appear, that is,

$$\begin{aligned} N_{311} &= N_{310} = N_{301} = N_{300}, \\ N_{221} &= N_{220}, \end{aligned} \tag{6}$$

as well as permutations hereof. In conjunction with eqs. (4), they imply that each $N_{j_1 j_2 j_3}$ is determined by the six numbers N_{311}, N_{131}, N_{113}, N_{221}, N_{212} and N_{122}. Moreover, within each triangle tower, these numbers are independent, because one can alter them separately by applying local changes in the geometry.

3. Extrinsic curvatures and light expansion rates

The main aim of this section is the derivation of an expression for the light expansion rate H of a spacelike $(d-2)$-dimensional surface S of constant time and constant radius in a simplicial product manifold of dimension four, in order to formulate necessary criteria for the presence of black holes in the quantum theory. We start by reminding the reader of the geometric meaning of trapped surfaces. For reasons of completeness, we then review the construction of the expansion rate in terms of the extrinsic curvatures of S and a suitably chosen spacelike hypersurface Σ for the case of a smooth d-dimensional manifold (M, g_{ab}), following the treatment in [21]. We then translate this to simplicial manifolds, starting with a construction of the extrinsic curvatures. The expansion rate is first computed for a three-dimensional triangulation, because the geometry of the situation is closely analogous to that in four dimensions, but much easier to visualize. We discuss the role of different types of simplicial building blocks and their effect in terms of the focussing and defocussing of light rays. As one would expect, the simplicial expressions for the expansion rates are subject to discretization ambiguities. We find that for specific choices of how the piecewise flat surface S traverses the top-dimensional building blocks of the triangulation, the formulas for the expansion rates in both three and four dimensions take on a particularly simple form which will be useful in numerical simulations.

3.1 Trapped surfaces

A central question in our attempt to set up a path integral for black-hole geometries is how one may recognize the existence of a black hole region or a horizon in the quantum geometry. One difficulty is that the usual definition of a black hole region is both a classical concept and highly non-local (for details, see [22] and references therein). To find the black hole region one has to know the entire spacetime manifold $\mathcal{M} = (M, g_{ab})$ and to find the entire causal past $J^-(\mathfrak{I}^+)$ of future null infinity $\mathfrak{I}^+$. The spacetime $\mathcal{M}$ is then said to contain a black hole

region if $\mathcal{M}$ does *not* coincide with the causal past of future null infinity. What motivates this definition is the fact that "nothing can escape from a black hole", and, in particular, nothing can escape to future null infinity. The event horizon is defined as the boundary of the black hole region, which in turn is defined as the complement of $J^-(\mathfrak{I}^+)$ in $\mathcal{M}$.

This definition is not suited for the formulation of a nonperturbative path integral in terms of dynamical triangulations, because there one can only work with spacetimes of finite volume. A more local criterion for a horizon or a black hole region is the existence of a so-called trapped surface. This also appears in other approaches to quantum geometry (see [23] and references therein), in classical general relativity in order to define "(nearly) isolated" horizons [24], as well as in "horizon finders" in numerical relativity (see, for example, [25]).

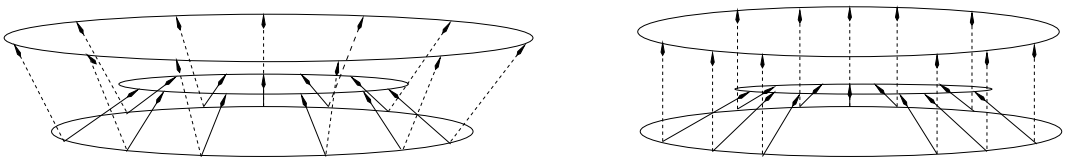

Figure 5: Inward- and outward-pointing light rays (solid and dashed arrows) outside a black hole region (left) and at an apparent horizon (right). Here we depict the situation in a (2+1)-dimensional spacetime, where the surface S (lower circle) is one-dimensional.

A trapped surface S is a compact spacelike surface of codimension two, with the following property. Consider future-directed null geodesics (i.e. light rays), which start off orthogonally from S. This can happen in two directions, called "inward-pointing" and "outward-pointing", see Fig. 5. (The distinction is natural since S is assumed to be closed, for instance, a sphere.) Light rays which point outward, say, can either diverge from or converge toward each other locally. This effect is measured by the outward-pointing expansion rate H_+, which can be either positive (for divergence), negative (for convergence) or vanishing. For a sphere in flat Minkowski space the expansion rate H_+ is everywhere positive and the analogous expansion rate H_- for inward-pointing light rays negative. However, for a sphere inside a black hole, even the outward-pointing light rays are bent inwards to such an extent that the expansion rate H_+ becomes negative too.

Consequently, one defines a *trapped surface* as a compact spacelike surface of codimension 2, whose expansion rates H_+ and H_- are both negative. If "negative" is replaced by "non-positive" one speaks of a *marginally trapped surface*. The outermost marginally trapped surface is called the apparent horizon (assuming certain technical conditions, which are unimportant here). Its geometry is

depicted in Fig. 5. One can show that its expansion rate H_+ vanishes everywhere.

For a Schwarzschild solution the apparent horizon coincides with the event horizon. Moreover, a marginally trapped surface is always contained in a black hole region, as defined above (see [22] and references therein for a precise formulation of the theorem). This holds also for spacetimes which do not fulfil the Einstein equations, but instead the condition $R_{ab}k^a k^b \geq 0$ for the Ricci tensor and all null vectors k^a. The latter is satisfied if the Einstein equations hold and if the matter satisfies the strong or weak energy condition.

These classical considerations motivate the replacement of the global characterization of black holes in terms of event horizons by the more local criterion that a trapped surface exist. The condition $R_{ab}k^a k^b \geq 0$ will not in general be satisfied by the spacetime geometries contributing to the nonperturbative path integral, because the individual path-integral histories are arbitrarily far away from classical solutions. However, one would expect to recover such a property at sufficiently large scales in an appropriate continuum limit of the theory. We will in the following concentrate on the condition $H_+ = 0$ as an indicator for the presence of black holes.

3.2 Continuum treatment

The light expansion rate H describes the expansion of a family of lightlike geodesics starting orthogonally from the $(d-2)$-dimensional surface S. It is defined by

$$H = \nabla_a p^a, \tag{7}$$

where ∇ is the Levi-Civita connection associated to the spacetime metric g_{ab} and p^a is the tangent vector field to a future-pointing null geodesic congruence starting off orthogonally from the surface S. In other words, p^a must satisfy

$$p_a p^a = 0, \qquad m_{ab} p^a_{|S} = 0, \tag{8}$$

and

$$p^a \nabla_a p^b = 0, \tag{9}$$

where m_{ab} is the metric induced on S by the spacetime metric g_{ab}. Embedding S into a spatial (constant-time) hypersurface Σ with future-pointing unit normal vector field n^a and calling $\pm q^a$ the (out- and inward-pointing) unit normals to S tangential to Σ, the $(d-2)$-dimensional metric is given by

$$m_{ab} = g_{ab} + n_a n_b - q_a q_b. \tag{10}$$

For later use, we also introduce the notation

$$h_{ab} = g_{ab} + n_a n_b \equiv m_{ab} + q_a q_b \tag{11}$$

for the induced metric on Σ. Note that m_{ab} is independent of the choice of Σ as long as the latter contains S. The general solution to eqs. (8) on S can then be written as

$$ {}^{\pm}p^a_{|S} = c_{\pm}(n^a \pm q^a), \tag{12} $$

with coefficients $c_{\pm}$ which are positive functions on S. As long as the functions $c_{\pm}$ are kept arbitrary, the general solution (12) does not depend on Σ in the sense that if one starts with another hypersurface Σ' and corresponding normal vectors n'^a and q'^a, one can always find functions $c'_{\pm}$ such that

$$ {}^{\pm}p^a_{|S} = c_{\pm}(n^a \pm q^a) = c'_{\pm}(n'^a \pm q'^a) = {}^{\pm}p'^a_{|S}. \tag{13} $$

Using the decomposition (10), we can compute the expansion rates $H_{\pm}$ for the in- and outward pointing light rays,

$$ \begin{aligned} H_{\pm} &= g^{ab}\nabla_a {}^{\pm}p_b \\ &= m^{ab}\nabla_a {}^{\pm}p_b + q^a q^b \nabla_a {}^{\pm}p_b - n^a n^b \nabla_a {}^{\pm}p_b \\ &= m^{ab}\nabla_a {}^{\pm}p_b - \left((c_{\pm})^{-1}\,{}^{\pm}p^b \mp q^b\right)(c_{\pm})^{-1}\ \left[{}^{\pm}p^a\nabla_a {}^{\pm}p_b\right] \pm q^a (c_{\pm})^{-1}\ \left[{}^{\pm}p^b\nabla_a {}^{\pm}p_b\right] \\ &= m^{ab}\nabla_a {}^{\pm}p_b. \end{aligned} \tag{14} $$

Going from the second to the third line, we have used eq. (12). The terms in square brackets vanish by virtue of relations (8) and (9). Noting that the covariant derivative is projected onto the surface S in the last line of (14), we can simplify the expansion rate further by using again the expression (12) for the vector fields ${}^{\pm}p^a$ on S,

$$ \begin{aligned} H_{\pm} &= m^{ab}\nabla_a\, c_{\pm}(n_b \pm q_b) \\ &= c_{\pm} m^{ab}\nabla_a n_b \pm c_{\pm} m^{ab}\nabla_a q_b + \left[m^{ab}(n_b \pm q_b)\right]\nabla_a c_{\pm} \\ &= c_{\pm}\left(-m^{ab}K_{ab} \mp k\right). \end{aligned} \tag{15} $$

The term in square brackets vanishes by definition of p_b, and in the third line we have defined the extrinsic curvature

$$ K_{ab} = -h^c_a \nabla_c n_b \tag{16} $$

of Σ in M, and the extrinsic curvature

$$ k_{ab} = -m^c_a h^d_b \nabla_a q_b \tag{17} $$

of S in Σ.

The last line of (15) shows that the signs of the expansion rates $H_{\pm}$ on S (which determine whether or not S is a trapped surface) are independent of the

prefactors $c_\pm$ introduced in eq. (12) which are always positive. Likewise, the condition $H_+ = 0$ for an apparent horizon does not depend on the choice of the constant-time surface Σ and therefore on c_+. Our reason for keeping track of the prefactors $c_\pm$ explicitly is the fact that in the quantum theory it may be convenient to monitor *integrated* expansion rates rather than local ones. If such an integration were performed over a surface S at a given time and radius and if the underlying geometry were exactly spherically symmetric, the expansion rate would be constant on S and the Σ-dependence of the integral would simply amount to an overall factor $c_\pm$. However, in situations without exact spherical symmetry, either in a smooth or a simplicial setting, it does matter a priori that the absolute magnitude of $H_\pm$ depends on $c_\pm$. If we define an "averagely (minimally) trapped surface" S in a generic geometry and for a specific hypermanifold Σ by

$$\mathfrak{H}_+(S) := \int_S H_+ \sqrt{\det m}\, \mathrm{d}S = 0, \tag{18}$$

where $\sqrt{\det m}\, \mathrm{d}S$ is the invariant volume element on S, the same condition will in general not hold for a different choice Σ' of the hypermanifold containing S, as was pointed out in [26]. The average expansion rate $\mathfrak{H}'_+$ may become positive, say, because the prefactor c'_+ which appears when one expresses $p^a = n^a + q^a$ in terms of the primed normals,

$$p^a = c'_+(n'^a + q'^a), \tag{19}$$

may be large in a region of positive H_+ (defined with respect to Σ) and small in a region of negative H_+, whereas the contributions from the two regions cancelled each other with respect to the unprimed spatial slice Σ.

It follows that some caution has to be applied when using the vanishing of averaged expansion rates as an indicator for the presence of black holes. This applies in particular to the case of simplicial manifolds which by their very nature can never be exactly spherically symmetric. Nevertheless, there are important situations – including the one considered here – where the vanishing of the integrated expansion rate, (18), *is* the relevant criterion for indicating the presence of an apparent horizon in the quantum theory. Firstly, we may use the preferred time foliation shared by all Lorentzian triangulated geometries in a quantum superposition to define the null geodesic congruence in terms of eq. (12) with $c_\pm \equiv 1$ and thus arrive at unique values for $H_\pm$. Second, as explained in the Introduction, we are interested in studying the path integral for approximately spherically symmetric geometries, in which case the variations across S of the expansion rate H_+ will not be large. Moreover, the surfaces Σ will be approximately spherically symmetric, and therefore the factors $c'_\pm$ connecting the expansion rates of two different (approximately spherically symmetric) surfaces Σ and Σ' will be

approximately constant, so that the case described above will generically not occur.

One can also formulate (local or integrated) criteria for the presence of trapped surfaces which depend quadratically on the expansion rates $H_{\pm}$. For example, a potential advantage of using the product H_+H_- is the fact that it is independent of the choice of the constant-time surface Σ [26]. A generic problem with such expressions in a simplicial approach is that they contain products of delta functions at the same point, and any regularization procedure is subject to a high degree of discretization ambiguity. Also, one generically cannot avoid an explicit dependence of the formulas on the local geometry of the triangulation, as opposed to mere counting of simplex types, which can be achieved for the linear expansion rates (c.f. Secs. 3.4 and 3.5 below). For these reasons, we will not pursue this possibility presently.

3.3 The case of piecewise linear manifolds

In this section we will develop an expression for the expansion rate for the case of a piecewise flat manifold, and will assume that both the constant-time surface Σ and the surface S are fibres with respect to the two product structures involved. The second of these assumption we will relax later on in Secs. 3.4 and 3.5, for reasons explained there. In order to apply formula (15) to the case of a piecewise linear manifold, we have to define an expression for the extrinsic curvature of a (piecewise linear) hypersurface in such a manifold. We begin by considering the extrinsic curvature K_{ab} of a $(d-1)$-dimensional constant-time hypersurface Σ_t (see the appendix for a definition) in a d-dimensional triangulation. Since the geometry of each d-simplex is flat and Minkowskian, a constant-time surface inside it is just a linear spacelike hypersurface (with boundaries) of this Minkowski space, and its extrinsic curvature vanishes. We will arrive at the same result (30) as reference [18]. However, our prefactors will differ from the ones obtained there, because we use different coordinates, which also appear as argument of the delta-function.

A key observation is that one can always imbed two adjacent d-dimensional simplices σ_1^d and σ_2^d isometrically into a common d-dimensional Minkowski space. It follows that the geometry across the $(d-1)$-dimensional boundary simplex $\sigma_{1\cap 2}^{d-1}$ separating the two adjacent simplices is flat. (This no longer holds for the (d–2)-dimensional subsimplices, on which the intrinsic curvature is concentrated.) In the common coordinate system, light rays crossing the $(d-1)$-dimensional timelike boundary simplex appear as straight lines, but a constant-time surface will in general be seen to have a "kink" there. This implies that its extrinsic curvature is concentrated on the $(d-2)$-dimensional intersections $\Sigma_t \cap \sigma_{1\cap 2}^{d-1}$ of the constant-time surface Σ_t with the $(d-1)$-dimensional timelike subsimplices.

The relevant geometry is therefore that of two linear spacelike hyperplanes in Minkowski space meeting in a kink (a (d–2)-dimensional linear submanifold) with a certain relative angle. The geometry is homogeneous in the directions along the kink. In the triangulation, we can ignore these directions as long as we stay away from the $(d-2)$-dimensional boundary simplices of the $(d-1)$-dimensional timelike subsimplex.

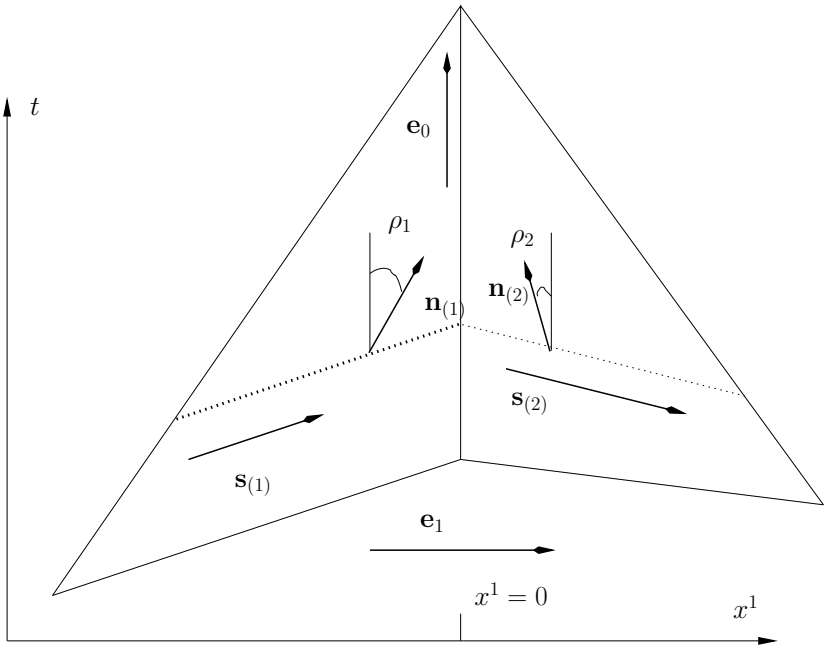

Figure 6: The geometry of two neighbouring d-simplices, seen in the two-dimensional plane perpendicular to the kink formed by the intersection of a constant-time surface (dotted lines) and their common $(d-1)$-boundary simplex. The common Minkowski coordinate frame is spanned by the unit vectors $\mathbf{e}_0$ and $\mathbf{e}_1$, with corresponding coordinates t and x^1. The origin of the spatial coordinate is taken to coincide with the location of the boundary simplex. Note that the normal vectors are perpendicular in a Lorentzian sense to the constant-time surface.

To analyze the geometry of the two-dimensional plane spanned by the two vectors normal to the kink, it is convenient to use the basis vectors $(\mathbf{e}_0)^a$ and $(\mathbf{e}_1)^a$ orthogonal to $\Sigma_t \cap \sigma^{d-1}_{1\cap 2}$ (see Fig. 6). By convention, $(\mathbf{e}_0)^a$ is future-directed and parallel to $\sigma^{d-1}_{1\cap 2}$ and $(\mathbf{e}_1)^a$ points from σ^d_1 to σ^d_2. Furthermore, we introduce corresponding Minkowski space coordinates (x^0, x^1), which measure the proper distances along the integral curves of $(\mathbf{e}_0)^a$ and $(\mathbf{e}_1)^a$ respectively. We define x^1 to be zero on $\sigma^{d-1}_{1\cap 2}$.

For the computation of the extrinsic curvature tensor we need the unit normals $n^a_{(1)}$ and $n^a_{(2)}$ to the two pieces $\Sigma^{(1)}_t$ and $\Sigma^{(2)}_t$ of the constant-time surface. Because

of their timelike nature, they can be written as

$$n^a_{(i)} = \cosh\rho_i\,(\mathbf{e}_0)^a + \sinh\rho_i\,(\mathbf{e}_1)^a, \tag{20}$$

where $\rho_i, i = 1, 2$ is the hyperbolic angle between $n_{(i)}$ and $\mathbf{e}_0$. Similarly, the (spacelike) unit tangent vectors to $\Sigma_t^{(1)}$ and $\Sigma_t^{(2)}$ (in the span of $(\mathbf{e}_0)^a$ and $(\mathbf{e}_1)^a$) are

$$s^a_{(i)} = \sinh\rho_i\,(\mathbf{e}_0)^a + \cosh\rho_i\,(\mathbf{e}_1)^a. \tag{21}$$

According to eq. (16), the extrinsic curvature is given by the projection onto Σ_t of the covariant derivative of the normal vector field, which in our Minkowski coordinates reduces to the usual coordinate derivative. In order to deal with the discontinuity of the normal vector field of Σ_t at the kink, we regularize it with the help of a family of smooth functions δ_ε which converge to the delta function as $\varepsilon \to 0$. The angle ρ between the time axis and the normal is then approximated by

$$\rho(x^1) = \rho_1 + \Delta\rho \int_{-\varepsilon}^{x^1} \delta_\varepsilon(x'^1)\ \mathrm{d}x'^1, \tag{22}$$

where $\Delta\rho = \rho_2 - \rho_1$. Projecting $-\nabla_a n^b(x^1)$ onto the hypersurface Σ_t with the projection operator $h^c_a := \eta^c_a + n_a n^c$ (where η_{ac} is the Minkowski metric), we obtain the extrinsic curvature

$$\begin{aligned} K^{ab}(x^1) &= -(\eta^{ac} + n^a(x^1)n^c(x^1))\nabla_c(\cosh\rho(x^1)\,(\mathbf{e}_0)^b + \sinh\rho(x^1)\,(\mathbf{e}_1)^b) \\ &= -(\eta^{ac} + n^a(x^1)n^c(x^1))\delta_\varepsilon(x^1)\,\Delta\rho\,(\mathbf{e}_1)_c\,s^b(x^1) \\ &= -\delta_\varepsilon(x^1)\,\Delta\rho\,\cosh\rho(x^1)\ s^a(x^1)\,s^b(x^1), \end{aligned} \tag{23}$$

where we have used that $\nabla_a x^1 = (\mathbf{e}_1)_a$.

For the calculation of the extrinsic curvature k^{ab} of the $(d-2)$-dimensional surface S in the surface Σ_t we proceed completely analogously. The constant-time surface Σ_t is a piecewise linear manifold, albeit a generalization of a simplicial manifold with more general building blocks than simplices. Again, we can now embed any two adjacent (d–1)-dimensional building blocks of the Σ_t-triangulation in a $(d-1)$-dimensional flat euclidean space. We choose the surface S as a linear $(d-2)$-surface inside each building block, possibly with a kink when one crosses from one building block to the other.

To analyze the geometry of S, consider the same two d-simplices as before and add a third basis vector $\mathbf{e}_2$ which is defined to be orthogonal to $\mathbf{e}_0$, $\mathbf{e}_1$ and to the intersection $S \cap \sigma^{d-1}_{1\cap 2}$. For $d = 3$ the intersection is just a point, and for $d = 4$ the geometry is homogeneous along the intersection. In the latter case, we complement the basis with a fourth normalized vector $\mathbf{e}_3$ orthogonal to the other three and thus tangential to $S \cap \sigma^{d-1}_{1\cap 2}$.

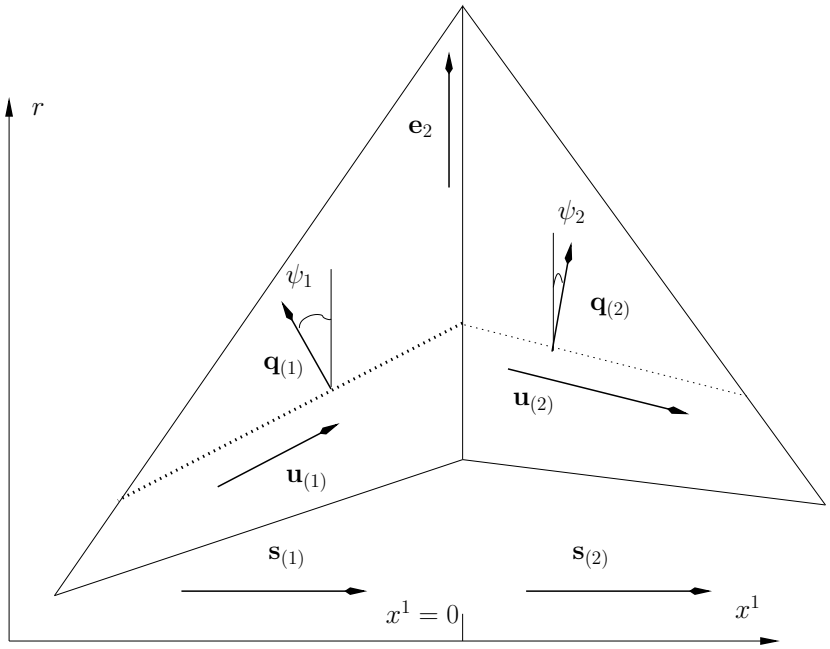

Figure 7: The geometry inside a constant-time hypersurface Σ_t. The figure illustrates various geometric quantities which appear in the calculation of the extrinsic curvature of the surface S (dotted line) in Σ_t. The surface S has been chosen straight inside either of the two neighbouring d-simplices, so that the only nontrivial contribution to the extrinsic curvature comes from the kink of S on the boundary between the two simplices. The vectors $\mathbf{s}_{(1)}$ and $\mathbf{s}_{(2)}$ may differ in the direction of $\mathbf{e}_0$ which is suppressed here.

The (outward-pointing) unit normals $q^a_{(i)}$ to $S^i := S \cap \sigma^d_i$ in Σ_t and those tangential vectors $u^a_{(i)}$ to S^i which lie in the plane spanned by $\mathbf{e}_2$ and $s_{(i)}$ may be written as

$$\begin{aligned} q^a_{(i)} &= \quad \cos\psi_i (\mathbf{e}_2)^a + \sin\psi_i \; s^a_{(i)}, \\ u^a_{(i)} &= -\sin\psi_i (\mathbf{e}_2)^a + \cos\psi_i \; s^a_{(i)}, \end{aligned} \tag{24}$$

where the angle ψ_i is the angle between the normal $q_{(i)}$ and the unit vector $\mathbf{e}_2$. Repeating our previous construction, we define an interpolating angle ψ by

$$\psi(x^1) = \psi_1 + \Delta\psi \int_{-\varepsilon}^{x^1} \delta_\varepsilon(x'^1) \; \mathrm{d}x'^1, \tag{25}$$

with $\Delta\psi = \psi_2 - \psi_1$. To determine the extrinsic curvature of S, we begin by calculating

$$\begin{aligned} \mathrm{D}_a q^b(x^1) &:= h_a{}^c(x^1)\, h^b{}_d(x^1) (\nabla_c q^d)(x^1) \\ &= \delta_\varepsilon(x^1)\, \Delta\psi \cosh\rho(x^1)\, s_a(x^1)\, u^b(x^1), \end{aligned} \tag{26}$$

where D_a denotes the induced covariant derivative in the submanifold Σ_t. This leads to the expression

$$\begin{aligned} k^{ab}(x^1) &= -m^{ac}(\mathrm{D}_c q^b)(x^1) = -(h^{ac}(x^1) - q^a(x^1)q^c(x^1))(\mathrm{D}_c q^b)(x^1) \\ &= -\delta_\varepsilon(x^1)\,\Delta\!\!\!/\psi\,\cosh\rho(x^1)\,\cos\psi(x^1)\;u^a(x^1)\,u^b(x^1). \end{aligned} \tag{27}$$

for the extrinsic curvature of S in Σ_t. Given the extrinsic curvatures of Σ_t and S, eqs. (23) and (27), it is now straightforward to apply the continuum formula (15) (with $c_+ = 1$) and calculate the expansion rates H_+ of outward-pointing light rays as

$$\begin{aligned} H_+(x^1) &= -k - m^{ab}K_{ab} \\ &= \delta_\varepsilon(x^1)(\Delta\!\!\!/\psi\,\cosh\rho(x^1)\cos\psi(x^1) + \Delta\!\!\!/\rho\,\cosh\rho(x^1)\cos^2\psi(x^1)). \end{aligned} \tag{28}$$

For the computation of the integrated expansion rate, it is convenient to introduce the variable p measuring the proper length along the orbits of u^a. From

$$u^a = -\sin\psi(\mathbf{e}_2)^a + \cos\psi(\sinh\rho\,(\mathbf{e}_0)^a + \cosh\rho\,(\mathbf{e}_1)^a) \tag{29}$$

we have $\mathrm{d}x^1 = \cosh\rho\cos\psi\,\mathrm{d}p$, and it follows that

$$H_+(p) = \delta_\varepsilon(p)(\Delta\!\!\!/\psi + \Delta\!\!\!/\rho\cos\psi(p)) \tag{30}$$

$$\stackrel{\varepsilon\to 0_+}{\to}\ \delta(p)(\Delta\!\!\!/\psi + \Delta\!\!\!/\rho\cos\psi_m) \tag{31}$$

where $\psi_m := \frac{1}{2}(\psi_1 + \psi_2)$ and we have assumed the functions δ_ε to be symmetric. For the case of a four-dimensional triangulation, by introducing a second (proper-length) coordinate x^3 along $(\mathbf{e}_3)^a$ the invariant volume element $\sqrt{\det m}\,\mathrm{d}S$ of S assumes the simple form $\mathrm{d}p\,\mathrm{d}x^3$. We can now easily integrate the expansion rate over a neighbourhood in S enclosing the set $S \cap \sigma^{d-1}_{1\cap 2}$ (that is, the support of the expansion rate in S), resulting in

$$\int_{\text{nbh.}} H_+ \mathrm{d}p\,\mathrm{d}x^3 = \mathrm{Vol}(\sigma^{\mathrm{d}-1}_{1\cap 2} \cap S)(\Delta\!\!\!/\psi + \Delta\!\!\!/\rho\cos\psi_m). \tag{32}$$

(For a three-dimensional triangulation, $d = 3$, we set $\mathrm{Vol}(\sigma^{\mathrm{d}-1}_{1\cap 2} \cap S) = 1$). In the integral over the whole surface S, the contributions from the $(d-3)$-dimensional building blocks simply add up to give the integral $\mathfrak{H}_+(S)$ of the expansion rate H_+ over the surface S,

$$\mathfrak{H}_+(S) = \int_S H_+\sqrt{\det m}\,\mathrm{d}S = \sum_{\sigma^{\mathrm{d}-1}\cap S} \mathrm{Vol}_{(\sigma^{\mathrm{d}-1}\cap S)}(\Delta\!\!\!/\psi + \Delta\!\!\!/\rho\cos\psi_m)_{(\sigma^{\mathrm{d}-1}\cap S)}. \tag{33}$$

When evaluating an expression like (33) for a dynamical triangulation it is inconvenient that the angles ρ_i and ψ_i defined by eqs. (20) and (24) depend on

the indexing of the d-simplices σ_1 and σ_2. This motivates the definition of new angles $\tilde{\rho}_i = (-1)^i \rho_i$ and $\tilde{\psi}_i = (-1)^i \psi_i$, in terms of which we have

$$\cosh\tilde{\rho}_i = -(\mathbf{e}_0)^a\, n^b_{(i)}\eta_{ab}, \quad \sinh\tilde{\rho}_i = (\tilde{\mathbf{e}}_1)^a_{(i)}\, n^b_{(i)}\eta_{ab}, \quad \Delta\rho = \tilde{\rho}_2 + \tilde{\rho}_1 \tag{34}$$

$$\cos\tilde{\psi}_i = (\mathbf{e}_2)^a\, q^b_{(i)}\,\eta_{ab}, \qquad \sin\tilde{\psi}_i = \tilde{s}^a_{(i)}\, q^b_{(i)}\,\eta_{ab}, \qquad \Delta\psi = \tilde{\psi}_2 + \tilde{\psi}_1, \tag{35}$$

where $(\tilde{\mathbf{e}}_1)^a_{(i)} = (-1)^i(\mathbf{e}_1)^a$ and $\tilde{s}^a_{(i)} = (-1)^i s^a_{(i)}$ are pointing toward the simplex σ^d_i for both $i{=}1$ and $i{=}2$. Furthermore, $\cos\psi_m$ may be written as

$$\cos\psi_m = \cos(\frac{1}{2}(\tilde{\psi}_1 - \tilde{\psi}_2)) = \cos(\frac{1}{2}(-\tilde{\psi}_1 + \tilde{\psi}_2)), \tag{36}$$

so that all quantities $\Delta\rho$, $\Delta\psi$, $\cos\psi_m$ appearing in the integrated expansion rate (33) are independent of the index i in σ^d_i.

3.4 The case of dynamical triangulations: 2+1 dimensions

In order to get an idea of what is involved in applying the framework of the previous section to the particular case of causal dynamical triangulations, we will first consider the simpler case of 2+1 dimensions. The triangulations take the form of fibrations over a two-dimensional base manifold, parametrized by a time and a radial coordinate. Our aim will be to derive a formula for the (integrated) expansion rate which is operationally simple to evaluate. In 2+1 dimensions the surface S on which we want to define the expansion rate H_+ is one-dimensional and H_+ is concentrated on the zero-dimensional vertices $v = \sigma^2 \cap S$ of the piecewise straight surface S. Following standard convention, we set the volume of these vertices to 1. Consider now a fibre S in a $[1_{T,in}, 1_{T,out}, 1_{T+1}]$-triangle tower.[6] Applying formula (33) for the integrated expansion rate gives

$$\mathfrak{H}_+(S) = -\mathfrak{k}(S) + \sum_{v\subset S} \Delta\rho(v)\cos\psi_m(v), \tag{37}$$

where

$$\mathfrak{k}\,(S) = \frac{\pi}{3}\,(N_{211} - N_{121}) \tag{38}$$

is the integrated extrinsic curvature of S in Σ_t. The values of the angles $\Delta\rho(v) = \tilde{\rho}_1(v) + \tilde{\rho}_2(v)$ and $\cos(\psi_m)(v) = \cos(\frac{1}{2}(\tilde{\psi}_1(v) - \tilde{\psi}_2(v)))$ contributing to eq. (37) can be read off the Tables 4 and 5. The term (38) is just a counting term which only depends on the total number of simplices of a certain type. This is not true for the remaining sum over vertices v in eq. (37). To evaluate it, we need to know not only

[6] Here T is an integer-valued time, and the lower-case t will henceforth denote a time value between T and $T+1$. The subscripts *in* and *out* refer to vertices with radial coordinates r_{in} and r_{out}, with $r_{in} < r_{out}$.

simplex	boundary simplex	$\tilde{\rho}$
$[3,1]$	$[2,1]$	$-\text{arsinh}\frac{1}{\sqrt{3+12\alpha}}$
$[1,3]$	$[1,2]$	$\text{arsinh}\frac{1}{\sqrt{3+12\alpha}}$
$[2,2]$	$[2,1]$	$\text{arsinh}\frac{1}{\sqrt{1+4\alpha}}$
$[2,2]$	$[1,2]$	$-\text{arsinh}\frac{1}{\sqrt{1+4\alpha}}$

Table 4: The angles $\tilde{\rho}$ per simplex type and per boundary simplex type contributing to the expansion rate in 2+1 dimensions. As usual in causal dynamical triangulations, we fix all spacelike edges to have a squared length $l_s^2 = a^2$ and all timelike edges to have $l_t^2 = -\alpha a^2$, where a is the so-called lattice spacing that will eventually be taken to zero. The number α parametrizes the (fixed) ratio between the length units in time and space directions.

$[i_{in,T}, j_{out,T}, k_{T\pm1}]$	$\tilde{\psi}$
$[2,1,1]$	$-\frac{\pi}{6}$
$[1,2,1]$	$\frac{\pi}{6}$
$[1,1,2]$	0

Table 5: The angles $\tilde{\psi}$ per simplex type in a triangle tower of type $[1_{T,in}, 1_{T,out}, 1_{T\pm1}]$ contributing to the expansion rate in 2+1 dimensions.

the numbers of the various simplex types but also how they are glued together. In other words, there exist pairs of triangulations with identical numbers N_{xyz} which nevertheless have different (integrated) expansion rates. This dependence on the local gluing information is caused by the factor $\cos\psi_m$ in (37), and can be traced back to our particular choice of the surface S. In the previous subsection, we assumed S to be straight inside each (constant-t hypersurface of a) three-simplex, as illustrated in Fig. 7. This leads to a coincidence of angles $\tilde{\rho}$ and $\tilde{\psi}$ at the intersection point $S \cap \sigma^{d-1}_{1\cap 2}$ between two three-simplices σ^3_1 and σ^3_2. We will adopt a different choice for the surfaces S which will simplify the functional form of the integrated expansion rate. We expect that this will speed up an eventual numerical implementation and also simplify any analytic considerations of the evaluation of the expectation value of the expansion rate in the path integral. The precise choice of S is a typical discretization ambiguity, which should not

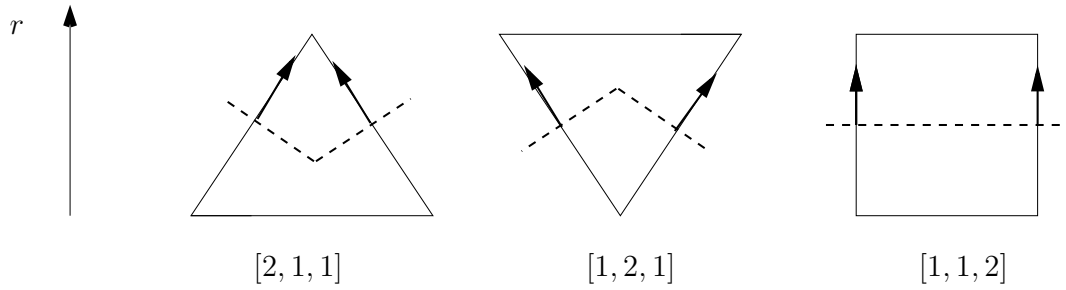

Figure 8: The "building blocks" which constitute our surfaces $\hat{S}$ of constant radius (dashed lines) inside the hypersurfaces Σ_t in 2+1 dimensions.

make any difference when we perform the continuum limit.[7] In the absence of an argument for which discretized choice of a "surface of constant radius" is more natural, we will adopt the simplest prescription, both here and in the four-dimensional case discussed in the next subsection.

Our alternative hypersurfaces $\hat{S}$ lie still within Σ_t, and are piecewise straight, but we arrange their straight segments to be dual to the edges of the original triangulation in Σ_t, as depicted in Fig. 8, so that the "kinks" of $\hat{S}$ no longer coincide with the points $S \cap \sigma^{d-1}_{1\cap 2}$. Since the angles $\Delta\psi$ are still the same as for the original surface S, the first term in the expansion rate (37) is unaffected, $\mathfrak{k}(\hat{S}) = \mathfrak{k}(S)$. However, since $\cos\psi_m$ is now always equal to 1, we obtain for the integrated expansion rate of $\hat{S}$

$$\mathfrak{H}_+(\hat{S}) = -\frac{\pi}{3}\,(N_{211} - N_{121}) - \{2\,\mathrm{arsinh}\frac{1}{\sqrt{3+12\alpha}}\,(N_{211} + N_{121})\,\} + 2\,\mathrm{arsinh}\frac{1}{\sqrt{1+4\alpha}}\,N_{112} \tag{39}$$

for a triangle tower of type $[1_{T,in}, 1_{T,out}, 1_{T+1}]$. For a triangle tower of type $[1_T, 1_{T+1,in}, 1_{T+1,out}]$ the first term, i.e. the extrinsic curvature of $\hat{S}$, is unchanged (apart from relabelling), whereas the terms coming from the extrinsic curvature of Σ_t change sign, leading to

$$\mathfrak{H}_+(\hat{S}) = -\frac{\pi}{3}\,(N_{121} - N_{112}) + \{2\,\mathrm{arsinh}\frac{1}{\sqrt{3+12\alpha}}\,(N_{121} + N_{112})\,\} - 2\,\mathrm{arsinh}\frac{1}{\sqrt{1+4\alpha}}\,N_{211}. \tag{40}$$

One thing to note about eqs. (39) and (40) is that the two terms in curly brackets have merely boundary character in the sense that they cancel when one considers

[7] Obviously such an assertion must eventually be verified.

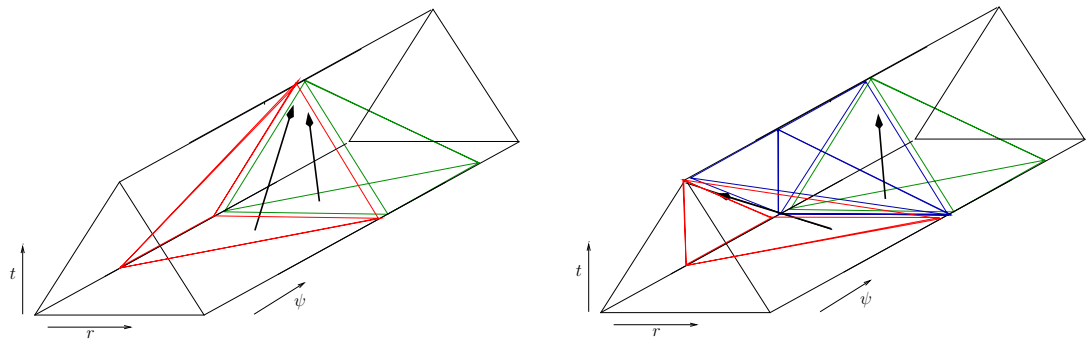

Figure 9: The effect of different three-simplices in a $[1_{T,in}, 1_{T,out}, 1_{T+1}]$-triangle tower on future-directed light rays. We only show the angular behaviour, which is relevant for calculating the expansion rate. Tetrahedra of type [3,1] focus light rays in the angular direction (left figure), whereas [2,2]-tetrahedra defocus them (right figure).

the expansion rate for more than one time step. For example, suppose we added the integrated expansion rates associated with two base triangles of type $[1_{T-1}, 2_T]$ and $[2_T, 1_{T+1}]$ with a common spacelike edge. Then the contributions from the two terms in curly brackets cancel each other, because the numbers of $[1_{T-1}, 3_T]$-tetrahedra in the first triangle tower equals the number of $[3_T, 1_{T+1}]$-tetrahedra in the second.

A second observation about the counting formulas (39) and (40) is that they have a direct geometric interpretation in terms of the focussing of light rays passing through the three-dimensional building blocks of the product triangulation. Let us call the fibre direction angular and the other spatial direction radial, and consider first a $[1_{T,in}, 1_{T,out}, 1_{T+1}]$-triangle tower. It contains both [3,1]-tetrahedra (which can be split into the subtypes [2,1,1] and [1,2,1]) and [2,2]-tetrahedra (of subtype [1,1,2]). The first term in (39), which depends on the difference $(N_{211} - N_{121})$, has a purely spatial origin and is determined by the triangulation of the spacelike edge tower. The second term (in curly brackets) in (39) gives a negative contribution, since a [3,1]-tetrahedron focusses light rays in the angular direction (see Fig. 9, left). It also focusses light rays in the radial direction. At any rate, since these effects cancel out for adjacent time slices as we have just explained, let us concentrate on the remaining term in (39). As illustrated in Fig. 9, the $[1, 1, 2]$-tetrahedra defocus light in the angular direction (thus accounting for their positive contribution to the integrated expansion rate on $\hat{S}$), and focus it in radial direction. In a $[1_T, 1_{T+1,in}, 1_{T+1,out}]$-triangle tower the focussing effects are exactly reversed: the $[1, 3]$-simplices defocus light rays (or timelike normal vectors) whereas the $[2, 1, 1]$-tetrahedra focus in angular and defocus in radial direction. We conclude that apart from the extrinsic curvature term $\mathfrak{k}$ of the (one-dimensional) surface $\hat{S}$ the expansion rate is determined by simply counting

the numbers of focussing and defocussing [2,2]-tetrahedra, associated with the $[1_{T-1}, 2_T]$ and $[2_T, 1_{T+1}]$-base triangles respectively, and taking their difference.

3.5 The case of dynamical triangulations: 3+1 = 2+2 dimensions

We will now generalize the treatment of the previous subsection to the case of a four-dimensional Lorentzian (i.e. causal) dynamical triangulation which is a product of a two-dimensional triangulated "r-t-plane" and a two-dimensional fibre, representing the angular directions. We will follow the same strategy as in the three-dimensional case to obtain a simple functional form for the expansion rate $\mathfrak{H}_+(S)$ which does not depend on detailed local gluing data.

For a (2+2)-dimensional triangulation, S is two-dimensional and $\mathfrak{H}_+(S)$ has distributional support on the one-dimensional edges $e = \sigma^3 \cap S$ in S. As before, if one defines the surface S to be a two-dimensional fibre in a triangle tower, it turns out that the expansion rate does not just depend on the numbers of the various simplex types in the triangle tower, because of the $\cos\psi_m$-terms in eq. (33). We will therefore choose an alternative surface $\hat{S}$, still inside the constant-time hypersurface Σ_t, but which intersects the two-dimensional building blocks contained in Σ_t orthogonally such that all $\cos\psi_m$-factors will be equal to one.

Note that in the $(2+1)$-dimensional case the surface $\hat{S}$ was related to the dual triangulation of Σ_t – the vertices of $\hat{S}$ were positioned at the barycentres of the triangles and rectangles which are the piecewise flat building blocks of Σ_t. (The vertices inside the rectangles did not appear explicitly, because they do not contribute to the extrinsic curvature of $\hat{S}$.) Also in 2+2 dimensions we will construct the surface $\hat{S}$ as part of the dual triangulation of the constant-time surface Σ_t. Recall from Sec. 2.3 that Σ_t consists of equilateral tetrahedra and triangular prisms with two equilateral triangular and three rectangular sides. To construct the dual triangulation, one places vertices at the barycentres of these tetrahedra and prisms, which one then joins by "dual" edges if they belong to neighbouring building blocks. These dual edges will orthogonally cross the boundary faces (triangles or rectangles shared by adjacent tetrahedra and/or prisms) exactly at their barycentres. The dual flat two-surfaces spanned between pairs of dual edges will therefore also intersect the two-dimensional faces of the Σ_t-triangulation orthogonally. Our surfaces $\hat{S}$ will by definition be built from those dual two-surfaces which extend in the angular directions.

The extrinsic curvature k of a surface $\hat{S}$ with respect to Σ_t is now concentrated on the dual edges. For some dual edges k vanishes, for example, for the dual edges in the $[2_T, 3_{T+1}]$-building blocks in a $[2_T, 1_{T+1}]$-triangle tower. We will now discuss each case in turn and compute its associated angle contribution $\Delta\psi$. Fig. 10 shows the three-dimensional flat building blocks that can appear in a constant-time hypersurface Σ_t, each with its corresponding "elementary" surface

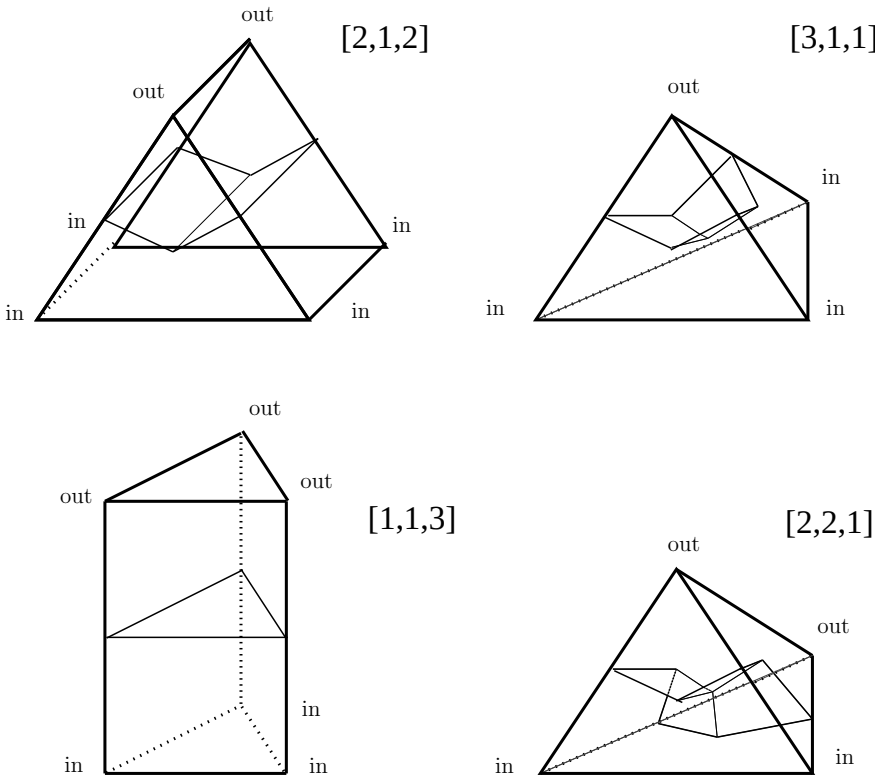

Figure 10: The elementary contributions of various three-dimensional building blocks in Σ_t to the two-dimensional surface $\hat{S}$ in a $[1_{T,in}, 1_{T,out}, 1_{T+1}]$-triangle tower. The cases not shown, associated with four-simplices of type [1,2,2] and [1,3,1], can be obtained by exchanging the role of the "in" and "out" vertices of the cases [2,1,2] and [3,1,1] respectively.

contributing to $\hat{S}$. There are essentially four different cases:

(i) The intersection of a four-simplex of type [2,1,2] or [1,2,2] with Σ_t is a prism. The surface $\hat{S}$ intersects both triangular faces and two of the rectangular faces. The dual edges in $\hat{S}$ which cross the rectangular faces do not carry any extrinsic curvature but the two edges which cross the triangular faces do. The angular difference between the two normals involved is $\Delta\psi = \pm\pi/3$.

(ii) The intersection of a four-simplex of type [3,1,1] or [1,3,1] with Σ_t is a tetrahedron. The surface $\hat{S}$ intersects three out of the four boundary triangles. Three dual edges connect the barycentre of the tetrahedron with the centres of these three triangles. The angular difference for each of the three dual edges is again $\Delta\psi = \pm\pi/3$.

(iii) The intersection of a four-simplex of type [1,1,3] with Σ_t is a prism. The surface $\hat{S}$ intersects the three boundary rectangles. Since the intersection

simplex	boundary simplex	$\tilde{\rho}$
$[4,1]$	$[3,1]$	$-\text{arsinh}\frac{1}{\sqrt{8}\sqrt{1+3\alpha}}$
$[3,2]$	$[3,1]$	$\text{arsinh}\frac{\sqrt{3}}{2\sqrt{1+3\alpha}}$
$[3,2]$	$[2,2]$	$-\text{arsinh}\frac{1}{\sqrt{6}\sqrt{1+2\alpha}}$

Table 6: The angles $\tilde{\rho}$ per simplex type and per boundary simplex type contributing to the expansion rate in 2+2 dimensions. For the time-reversed simplices we have $\tilde{\rho}([i,k]) = -\tilde{\rho}([k,i])$.

surface is a single flat triangle parallel to the triangular boundaries of the prism, there are no contributions to the extrinsic curvature.

(iv) The intersection of a four-simplex of type [2,2,1] with Σ_t is a tetrahedron. The surface $\hat{S}$ intersects all four boundary triangles. However, since there are two types of dual edges which contribute with angles of opposite sign, the net contribution to the extrinsic curvature vanishes.

The extrinsic curvature of Σ_t with respect to the four-dimensional triangulation is concentrated on the two-dimensional faces of the Σ_t-building blocks. The angles $\tilde{\rho}$ needed to calculate this quantity are listed in Table 6. The surface $\hat{S}$ intersects the two-dimensional faces orthogonally, and the extrinsic curvature term $K^{ab}m_{ab}$ appearing in the expansion rate (c.f. eq. (28)) therefore has distributional support on these one-dimensional intersections. Note that they do not coincide with the dual edges contained in $\hat{S}$, but are positioned transversally to them. To determine the integrated extrinsic curvatures K we still need to calculate the lengths of these intersections, which is straightforward and will lead to an explicit t-dependence of the expansion rate. Similarly, to obtain the extrinsic curvatures k one has to multiply the angular differences $\Delta\psi$ with the lengths of the associated dual edges. The final result for the integrated expansion rate for a $[1_{T,in}, 1_{T,out}, 1_{T+1}]$-triangle tower and a surface $\hat{S}$ in a constant-time surface Σ_t is given by

$$\begin{aligned}\mathfrak{H}_+(\hat{S}) = a\Big((1-t)\frac{\pi}{2\sqrt{6}}(N_{131}-N_{311}) + t\frac{\pi}{3}(N_{122}-N_{212}) + \\ \Big\{(1-t)(-\sqrt{3})\,\text{arsinh}(\frac{1}{\sqrt{8}\sqrt{1+3\alpha}})(N_{311}+N_{131}+\frac{4}{3}N_{221})\Big\} + \\ 3t\,\text{arsinh}(\frac{1}{\sqrt{6}\sqrt{1+2\alpha}})\,N_{113} +\end{aligned}$$

$$\Big[((1-t)\frac{2}{\sqrt{3}}\mathrm{arsinh}(\frac{\sqrt{3}}{2\sqrt{1+3\alpha}}) - 2t\,\mathrm{arsinh}(\frac{1}{\sqrt{6}\sqrt{1+2\alpha}}))(N_{212}+N_{122})\Big]\Big). \tag{41}$$

Similarly, for a $[1_{T-1}, 1_{T,in}, 1_{T,out}]$-triangle tower and a surface $\hat{S}$ in a constant-time surface $\Sigma_{(T-1)+t}$ one obtains

$$\begin{aligned}\mathfrak{H}_+(\hat{S}) = a\Big(&t\frac{\pi}{2\sqrt{6}}(N_{113}-N_{131}) + (1-t)\frac{\pi}{3}(N_{212}-N_{221}) - \\ &\Big\{t(-\sqrt{3})\,\mathrm{arsinh}(\frac{1}{\sqrt{8}\sqrt{1+3\alpha}})(N_{131}+N_{113}+\frac{4}{3}N_{122})\Big\} - \\ &3(1-t)\,\mathrm{arsinh}(\frac{1}{\sqrt{6}\sqrt{1+2\alpha}})\,N_{311} - \\ &\Big[(t\frac{2}{\sqrt{3}}\mathrm{arsinh}(\frac{\sqrt{3}}{2\sqrt{1+3\alpha}}) - 2(1-t)\,\mathrm{arsinh}(\frac{1}{\sqrt{6}\sqrt{1+2\alpha}}))(N_{221}+N_{212})\Big]\Big).\end{aligned} \tag{42}$$

These formulas have the desired form of depending only on counting-variables for the simplices in a given triangle tower. As before, one can achieve a further simplification by adding contributions from successive time layers. Consider two triangle towers which are joined by a spacelike edge in the base manifold. If one chooses the two constant-time surfaces at which the contributions to the extrinsic curvature are evaluated to be at times $(T+t)$ and $(T-1)+(1-t) = (T-t)$, the terms in the curly brackets in (41) and (42) will cancel each other because the numbers of the various types of $[4_T, 1_{T+1}]$-simplices equal those of the corresponding $[1_{T-1}, 4_T]$-simplices. An obvious and symmetric choice that achieves this cancellation over a larger number of time steps is therefore to evaluate the expansion rate always at half-integer times.

To summarize, the expansion rate in 2+2 dimensions is again a sum of terms coming from the extrinsic curvature k of $\hat{S}$ and of the extrinsic curvature K of Σ_t. The former are already determined by the triangulation of the spacelike edge tower, namely, the partitioning of the $[4,1]$-simplices into the subtypes $[3,1,1]$, $[1,3,1]$ and $[2,2,1]$, and similarly for the [1,4]-simplices. In analogy with what happened in the (2+1)-dimensional case, the contribution from the curvature K is determined by the distributions of the simplicial building blocks of type $[3,2]$ and $[2,3]$. In a $[1_{T,in}, 1_{T,out}, 1_{T+1}]$-triangle tower the $[1,1,3]$-simplices defocus light rays and in a $[1_{T-1}, 1_{T,in}, 1_{T,out}]$-triangle tower the $[3,1,1]$-simplices focus light rays in the angular directions. This is similar to the behaviour of the $[1,1,2]$- and $[2,1,1]$-tetrahedra in 2+1 dimensions. Note also that the contributions from the terms in square brackets in (41) and (42) are small, because the (absolute value of the) prefactor is small (< 0.016 for $\alpha > 7/12$, which is the range usually

considered [4]). This is due to the fact that the extrinsic curvature terms coming from the $[3,1]$- and the $[2,2]$-boundary simplex have opposite signs.

4. Dynamical triangulation of a black hole

In this section we will explain how to construct a black-hole geometry in the formulation of causal dynamical triangulations. This is not only a good exercise in translating metric data (which still depend on a coordinate choice) into invariant geometric data, but may also be helpful in deciding on the boundary conditions for a path integral over black-hole geometries. It should be kept in mind that unlike in Regge calculus [27] we are working with simplices of *fixed* squared edge lengths a^2 and $-\alpha a^2$ for the spacelike and timelike edges respectively. As is well known, these fixed building blocks are not well suited for approximating arbitrary smooth geometries pointwise, as may be desirable in a numerical study of *classical* Einstein gravity. Instead, as already discussed in the Introduction, the application we have in mind here is a nonperturbative quantum superposition of spacetime geometries, with classical properties emerging only on sufficiently coarse-grained scales.

This property of dynamical triangulations prevents us from approximating a given smooth manifold exactly, even in the limit as the lattice spacing $a \to 0$. For example, it is not possible to obtain a tesselation of three-dimensional flat euclidean space using equilateral tetrahedra. Nevertheless, one can usually arrange that geometric quantities – for example, the curvature scalar – when integrated or averaged over sufficiently large patches match certain prescribed values[8], and this is what we will employ in the following.

The explicit construction of a triangulated black hole can be simplified greatly by an appropriate choice of coordinates in the continuum. Since causal dynamical triangulations come with a distinguished notion of proper time, measuring the invariant distance between hypersurfaces of constant time, it is natural to start with coordinates in a proper-time gauge, where the lapse function is equal to one everywhere. In the following subsections we will describe the relevant black-hole configuration (given by the Kottler solution), identify appropriate coordinates for it, and construct a triangulation for the r-t-plane of this geometry. The latter serves as base space for a full four-dimensional triangulation which can be constructed as a triangulation of product type. By its very construction our simplicial rendering of the black-hole geometry is highly nonunique, and should merely be regarded as an illustration of how it can be achieved.

[8]This simple strategy does not work for quantities which are non-negative, for example, the square R^2 of the Riemann curvature scalar. In such cases, one may need to perform a finite "renormalization" or use a more sophisticated way of averaging. Ultimately any such prescription must be motivated by physical considerations.

4.1 The Kottler solution

Since the method of dynamical triangulations requires a positive (bare) cosmological constant, the relevant spherically symmetric black-hole configuration is not the Schwarzschild solution, but the so-called Kottler solution which describes a black hole in a de-Sitter background with a positive cosmological constant Λ. The line element of the Kottler solution in Schwarzschild-like coordinates (t, r, θ, ϕ) is given by [28]

$$\begin{aligned} ds^2 &= -\left(1 - \frac{2M}{r} - \frac{r^2}{L^2}\right) dt^2 + \left(1 - \frac{2M}{r} - \frac{r^2}{L^2}\right)^{-1} dr^2 + r^2 d\Omega^2 \\ &=: -f(r)dt^2 + f(r)^{-1}dr^2 + r^2 d\Omega^2, \end{aligned} \tag{43}$$

where M is a mass parameter, L a length parameter defined by $L^2 = \frac{3}{\Lambda}$, and $d\Omega^2$ the volume element of the unit two-sphere. Apart from the physical singularity at $r = 0$ there are two coordinate singularities at the positive real roots of $f(r)$ (if $M < L/\sqrt{27}$, as we will assume from now on), corresponding to the black-hole horizon and the cosmological horizon of the de-Sitter background. The latter is positioned at $r = L$ if the mass M vanishes. The maximal analytical continuation of the spacetime geometry (43) includes infinitely many black-hole and cosmological horizons, but for our present purposes we will only be interested in a region inside the cosmological horizon which contains a single black hole.

To facilitate the translation of the metric data of the Kottler solution to a dynamical triangulation, it is convenient to work in a proper-time gauge, that is, use coordinates in which the lapse function is equal to 1. A particular set of such coordinates are the Painlevé-Gullstrand (PG) coordinates (τ, r, θ, ϕ) [29, 30], in terms of which the metric (43) assumes the form

$$ds^2 = -d\tau^2 + \left(dr + \sqrt{1 - f(r)}\, d\tau\right)^2 + r^2 d\Omega^2. \tag{44}$$

We observe that the lapse function is equal to 1, but the shift N_r in the radial direction is nonvanishing, $N_r = \sqrt{1 - f}$. One can also find coordinates with the same constant-time surfaces as in (44) and $N_r = 0$, but it turns out that for our discussion keeping the nonvanishing shift function is more convenient. A remarkable property of the PG-coordinates is the fact that the induced constant-time surfaces Σ_τ are flat Euclidean three-spaces. Our triangulated black hole will have the form of constant-time surfaces represented by three-dimensional spatial triangulations which are (approximately) flat and connected to each other using the information contained in the shift function N_r.

4.2 Triangulation of the base manifold

Next, we will triangulate the geometry induced on the hypersurface $\{\theta = const.,\ \phi = const.\}$, which is parametrized by a coordinate pair (τ, r). The radial coordinate r is a "proper-length" coordinate in the same sense in which τ is a proper-time coordinate. It is therefore natural to identify (a rescaled version of) τ with the discrete time T inherent in a causal dynamical triangulation and (a rescaled version of) r with a discrete coordinate R along the one-dimensional spacelike triangulation Σ_T. We can introduce a discrete radial coordinate R simply by taking a triangulated half-line[9] and enumerating its vertices by 0, 1, 2, ..., starting from the left-most vertex, say. Since spatial edges by definition have a geodesic length a, discrete and continuous radii are related by $r = a\,R$. Similarly, one finds $\tau = a\sqrt{\alpha+1/4}\,T$ for the relation between the discrete and continuous times.

Consider now a spacelike edge e in Σ_T whose centre has radial coordinate R_T. If we want to erect a $[2_T, 1_{T+1}]$-triangle over this edge we must decide which vertex in the next constant-time line Σ_{T+1} the tip of the triangle should be connected to. Because the vector $\vec{\mathbf{n}}$ pointing from the middle of the edge e to the tip of the triangle is normal to the hypersurface Σ_T, the displacement of this top vertex along Σ_{T+1} from the position R_T on Σ_T is determined by the shift N_r. Explicitly, the position R_{T+1} of the top vertex is given by

$$R_{T+1} = R_T - N_r(a\,R_T)a^{-1}\Delta\tau \equiv R_T - N_r(a\,R_T)\sqrt{\alpha+1/4}, \tag{45}$$

where $\Delta\tau$ is the modulus of the length of the vector $\vec{\mathbf{n}}$. In order to construct an explicit triangulation, (45) must be approximated by integers. Whichever prescription one chooses, the following cases may occur when calculating the locations of the tips of $[2,1]$-triangles:

(o) The normal vectors $\vec{\mathbf{n}}_1$ and $\vec{\mathbf{n}}_2$ of two neighbouring $[2,1]$-triangles cross within the slice $\Delta T = 1$. For this to happen, $\partial_r N_r$ must be positive and $\partial_r N_r > 1/\Delta\tau$ i.e. the geometry must vary on scales smaller than a. For the Kottler solution this does not occur as long as $a \ll L = \sqrt{3/\Lambda}$.

(i) The tips of two neighbouring $[2,1]$-triangles coincide. In this case the (component in r-direction of the) extrinsic curvature is positive since the normals converge toward each other.

(ii) The tips of two neighbouring $[2,1]$-triangles with base in Σ_T are one or more edges apart in Σ_{T+1}. In this case, we fill the space between the two $[2_T, 1_{T+1}]$-triangles with the appropriate number of $[1_T, 2_{T+1}]$-triangles. The

[9] In numerical simulations, there will always be a maximal radius R_{max}, because of the finiteness of the spacetime volume.

extrinsic curvature is zero when a single upside-down triangle is inserted, and negative otherwise.

(iii) The position R_{T+1} assumes negative values. For the Kottler solution this happens whenever the discrete radial coordinate R_T satisfies

$$(R_T)^3 < \frac{1}{a^3}\,\frac{2M(\Delta\tau)^2}{1-\frac{(\Delta\tau)^2}{L^2}} \approx \frac{2M(\Delta\tau)^2}{a^3} = \frac{2M}{a}(\alpha+\frac{1}{4}), \tag{46}$$

where the approximation in the second step is justified because of $a \ll L$. In this case we simply omit the $[2,1]$-triangles. This way one obtains a spacetime boundary which is effectively spacelike (because there are far more spacelike than timelike edges), as illustrated by Fig. 11. It corresponds to the spacelike singularity of the Kottler solution at $r=0$.

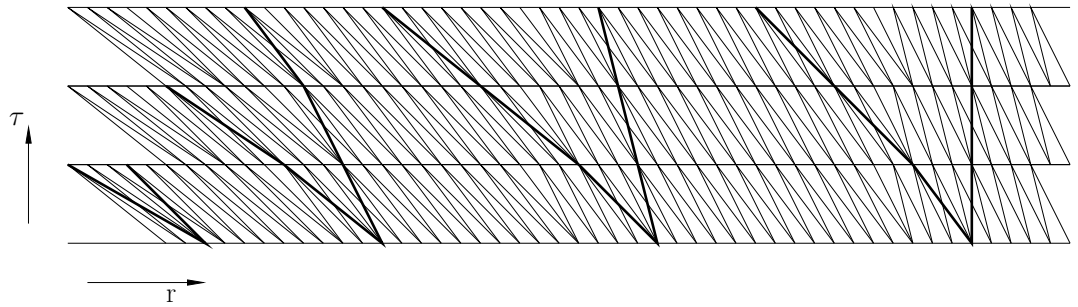

Figure 11: Example of a dynamically triangulated black hole. The thick lines correspond to light rays, and the vertical light ray on the right runs along the horizon.

Fig. 11 shows the typical features of a dynamically triangulated black hole: approaching smaller radii, the tips of the $[2,1]$-triangles get dragged more and more toward the centre of the black hole (left in the figure). Similarly, a freely falling particle which starts at some radius r on a surface Σ_T and normal to it, will roughly follow the direction of the timelike normals of these triangles and finally fall into the singularity. The horizon in this picture is located at the radius r_H at which the line $r = const.$ is lightlike.

4.3 Triangulation of the four-dimensional manifold

Finally, we will sketch how to construct a four-dimensional dynamically triangulated black-hole geometry by suitably triangulating the fibres F over one of the triangulated base spaces B of the previous section. In other words, one has to

provide a triangulation of the triangle towers $\sigma \times F$ for all triangles σ of the base space, as described in Sec. 2.3. Since there is no triangulation which is exactly spherically symmetric, the spherical symmetry of the Kottler solution can be implemented at most in an averaged sense. We will formulate conditions on the numbers of various simplex types in the fibres which must be satisfied in order that the fibre triangulations can be made homogeneous on large scales $l \gg a$. We will not spell out how these building blocks should be distributed over the fibres in a maximally uniform manner.

Since the spatial hypersurfaces Σ_τ of the metric (44) are flat, the radii r provide a direct measure of the areas of the associated two-spheres $\{\tau = const., r = const.\}$. This implies that a vertex tower with radial coordinate R should contain (approximately) $c_1 R^2$ triangles, where $c_1 \approx 4\pi/A_\Delta$ is of order 1, and A_Δ is the area of a spatial triangle in units of a. This consideration fixes the number of triangles in a vertex tower and therefore the numbers of $[3_R, 1_{R+1}]$- and $[1_R, 3_{R+1}]$-tetrahedra in a spatial edge tower located between the radii R and $R+1$. What remains to be specified is the number of $[2_R, 2_{R+1}]$-tetrahedra in the spatial edge tower. This can be done by demanding that the (absolute value of the) integrated intrinsic curvature of the edge tower be minimal, i.e. as close to zero as possible.

Fixing thus the numbers of simplices appearing in the triangulated surfaces Σ_T of constant time implies that also the numbers of $[4_T, 1_{T+1}]$- and $[1_T, 4_{T+1}]$-simplices (in the $[2_T, 1_{T+1}]$- and $[1_T, 2_{T+1}]$-triangle towers respectively) of the four-dimensional triangulation are fixed. Similarly, the number of $[1_{T,in}, 1_{T,out}, 3_{T+1}]$-simplices in a $[2_T, 1_{T+1}]$-triangle tower is already specified by the volume of the vertex tower over the tip of the triangle vertex with time coordinate $T+1$. All we are left with are the numbers of $[2_{T,in}, 1_{T,out}, 2_{T+1}]$- and $[1_{T,in}, 2_{T,out}, 2_{T+1}]$-simplices or, equivalently, the numbers of $[2_T, 2_{T+1}]$-simplices in the timelike edge towers $[1_T, 1_{T+1}]$. These numbers can also be determined by demanding a vanishing integrated four-dimensional intrinsic curvature scalar, see [19] for details.

5. Summary and outlook

In this paper we have derived an explicit expression for the expansion rate of light rays for a simplicial manifold of the kind that occurs in the sum over geometries in the causal dynamical triangulations approach to quantum gravity. Its prime intended use is in a horizon finder in the quantum theory. The vanishing of the *integrated* version of the expansion rate is an indicator for an apparent horizon in situations where the geometry along the angular directions is homogeneous at sufficiently large scales. Our non-integrated expression for the expansion can also be used in more general situations, but a numerical horizon search would be considerably more involved, because the expansion rate would have to be

monitored not just as a function of radius and time, but also of the two angular directions.

As a first step towards understanding the role of black holes in nonperturbative quantum gravity we suggest to investigate the situation where the geometric configurations are approximately spherically symmetric. In practice, one would first search for the formation of an apparent horizon as function of the boundary conditions. This will involve monitoring the integrated expansion rate $\mathfrak{H}_+(\hat{S})$ given in eqs. (39) and (40) as a function of the discrete radius and time coordinates of the triangulated base manifold. One will have to work out how the local Monte Carlo moves [4] change the counting variables appearing in $\mathfrak{H}_+(\hat{S})$ in a small neighbourhood of triangle towers. In case one manages to find evidence for an apparent horizon, one will try to understand whether also other large-scale properties of the geometry match those of a (classical) black hole. Ultimately, one is of course interested in the quantum deviations from the classical geometry, especially near the horizon and for very small radii, to obtain further insights into a possible quantum origin of (horizon) entropy and a quantum resolution of the central singularity. These are doubtless ambitious goals, but with some luck and ingenuity they may just be within reach of our computational means.

Acknowledgments

B.D. thanks the German National Merit Foundation for financial support and the Institute for Theoretical Physics of Utrecht University for hospitality. R.L. acknowledges support by the Netherlands Organisation for Scientific Research (NWO) under their VICI program.

Appendix

In this appendix, we define the concept of affine coordinates for flat simplices, and use them to describe hypersurfaces Σ_t of constant time, as well as the surfaces S used in the computation of the extrinsic curvatures in Sec. 3.3. For illustrative purposes, we also perform a simple model calculation for $d=2$.

For the computation of various geometrical quantities like the angles (34) and (35) appearing in the expansion rate (33), it is very convenient to introduce affine or barycentric coordinates (see, for instance, [31]). Consider a d-simplex σ^d embedded into d-dimensional Minkowski space. Let the vectors $\vec{v}_j$, $j=1,\ldots,d+1$ point from the (arbitrarily chosen) origin to the $(d+1)$ vertices of the simplex. One can then describe an arbitrary point P in σ^d as the centre of mass of $(d+1)$

appropriately chosen masses $m^j \geq 0$ located at the vertices of the simplex,

$$P = \sum_{j=1}^{d+1} m^j \vec{v}_j, \tag{47}$$

where the sum of the coordinates m^j is normalized to

$$\sum_{j=1}^{d+1} m^j = 1. \tag{48}$$

An affine vector can be defined by the difference of two points P_1 and P_2,

$$\overrightarrow{P_1 P_2} = \sum_{j=1}^{d+1} (m_2^j - m_1^j)\vec{v}_j. \tag{49}$$

The sum of the vector components $y^j := (m_2^j - m_1^j)$ in (49) vanishes because of the normalization (48). We can therefore replace the vectors $\vec{v}_j$ in (49) by the affine basis vectors

$$\mathbf{a}_j := \vec{v}_j - \frac{1}{d+1} \sum_{k=1}^{d+1} \vec{v}_k, \tag{50}$$

which are overcomplete due to $\sum_j \mathbf{a}_j = 0$.

In order to express the metric in affine coordinates we still need a basis of one-forms dual to $\{\mathbf{a}_j\}$. Because of the overcompleteness of the vector basis, the dual basis $\{\mathbf{a}^j\}$ is defined by

$$\langle \mathbf{a}_j, \mathbf{a}^k \rangle = \tilde{\delta}_j^k := \delta_j^k - \frac{1}{d+1}, \tag{51}$$

where $\tilde{\delta}_j^i$ is the projector onto the space of affine coordinates, i.e. it projects an arbitrary $(d+1)$-tuple of numbers into one whose sum vanishes and it acts as the identity on tuples $(y^1, \ldots, y^{d+1})$ which have a vanishing sum $\sum y^j = 0$.

The (Minkowski) metric components of a simplex in affine coordinates take the form [31]

$$\tilde{\eta}_{ij} = -\frac{1}{2} l_{km}^2 \tilde{\delta}_i^k \tilde{\delta}_j^m, \tag{52}$$

where l_{ij}^2 is the squared geodesic length of the edge between the i-th and j-th vertex. The metric two-form is then given by $\eta = \tilde{\eta}_{ij} \mathbf{a}^i \mathbf{a}^j$. Since the $\tilde{\delta}_j^i$'s on the right-hand side of (52) are projections onto the space of affine coordinates they can be replaced by ordinary Kronecker symbols δ_j^i if (52) is contracted with coordinate tuples that already fulfill the affine coordinate condition (i.e. sum

up to zero). One can check eq. (52) by contracting it with the simplex edges $e_{(ij)} := \vec{v}_j - \vec{v}_i = \mathbf{a}_j - \mathbf{a}_i$ which gives the expected result

$$\eta(e_{(ij)}, e_{(ij)}) = l_{ij}^2. \tag{53}$$

With the help of the barycentric coordinates one can give an easy characterization of the fibres with respect to the two different product structures introduced in Sec. 2, namely, the constant-time hypersurfaces Σ_t and the surfaces S of codimension two. First, consider a d-simplex of type $[N_T, N_{T+1}]$, that is, a simplex having N_T vertices in the hypersurface Σ_T and N_{T+1} vertices in the neighbouring surface Σ_{T+1}. The barycentric coordinates $(m^1, \ldots, m^{d+1})$ of any point in the intersection of Σ_{T+t}, $0 \leq t \leq 1$, and the d-simplex $[N_T, N_{T+1}]$ satisfy

$$\sum_{j=1}^{N_T} m^j = 1 - t = 1 - \sum_{j=N_T+1}^{d+1} m^j. \tag{54}$$

This condition describes a linear subspace whose points have a "constant distance" from the T- and the $(T+1)$- vertices.

A surface S can be characterized in an analogous manner. Consider a d-simplex of type $[N_{T,in}, N_{T,out}, N_{T+1}]$, with $N_{T,in}$ vertices in the inner and $N_{T,out}$ in the outer vertex tower at time T and N_{T+1} vertices in the vertex tower at time $T+1$. (We use "inner" and "outer" merely as labels to distinguish between the two vertex towers at equal time.) Then the intersection of the d-simplex with the surface S is the set of points having "constant distance" to these three set of vertices,

$$\sum_{j=1}^{N_{T,in}} m^j = r, \qquad \sum_{j=N_{T,in}+1}^{N_{T,in}+N_{T,out}} m^j = s, \qquad \sum_{j=N_{T,in}+N_{T,out}+1}^{d+1} m^j = t, \tag{55}$$

where $r + s + t = 1$. Obviously these points also fulfil eq. (54), which shows that S is a submanifold of Σ_{T+t}.

To illustrate the construction, consider the simple case of a two-dimensional Lorentzian triangulation containing a spacelike hypersurface Σ_{T+t}. We want to calculate the angles $\tilde{\rho}$ defined in (34) to compute the extrinsic curvature of Σ_{T+t}. Take a $[2_T, 1_{T+1}]$-triangle and introduce barycentric coordinates (m^1, m^2, m^3). From eq. (52), the components of the Minkowski metric in affine coordinates are given by

$$\tilde{\eta}_{ij} = \begin{cases} 0 & \text{for } i = j, \\ -\frac{a^2}{2} & \text{for } e_{(ij)} \text{ a spacelike edge}, \\ \frac{\alpha a^2}{2} & \text{for } e_{(ij)} \text{ a timelike edge}, \end{cases} \tag{56}$$

where we have assumed that the metric is contracted with affine coordinate tuples only. The tangential vector to Σ_{T+t} is $s = c_s(1, -1, 0)$, with a normalization

constant c_s. Orthogonal to this and future-directed is the normal vector $n = c_n(-\frac{1}{2}, -\frac{1}{2}, 1)$. If we take as the timelike boundary simplex the edge $e_{(1,3)}$, the future-directed vector parallel to it is $\mathbf{e}_0 = c_0(-1, 0, 1)$. Lastly, orthogonal to $\mathbf{e}_0$ and pointing into the 2-simplex is the vector

$$\tilde{\mathbf{e}}_1 = c_1(\frac{-1-2\alpha}{2\alpha}, 1, \frac{1}{2\alpha}). \tag{57}$$

Application of the formulas (34) to the (normalized) vectors $\mathbf{e}_0$, $\tilde{\mathbf{e}}_1$ and n leads to the angle

$$\tilde{\rho}_{[2,1]} = -\text{arsinh}(\frac{1}{2\sqrt{\alpha}}). \tag{58}$$

By an analogous calculation for an "upside-down" triangle $[1_T, 2_{T+1}]$ one obtains the corresponding angle $\tilde{\rho}_{[1,2]} = -\tilde{\rho}_{[2,1]}$.

References

[1] J. Ambjørn and R. Loll: *Non-perturbative Lorentzian quantum gravity, causality and topology change*, Nucl. Phys. B 536 (1998) 407-434 [hep-th/9805108].

[2] J. Ambjørn, J. Jurkiewicz and R. Loll: *A nonperturbative Lorentzian path integral for gravity*, Phys. Rev. Lett. 85 (2000) 924-927 [hep-th/0002050].

[3] J. Ambjørn, J. Jurkiewicz and R. Loll: *Non-perturbative 3d Lorentzian quantum gravity*, Phys. Rev. D 64 (2001) 044011 [hep-th/0011276].

[4] J. Ambjørn, J. Jurkiewicz and R. Loll: *Dynamically triangulating Lorentzian quantum gravity*, Nucl. Phys. B 610 (2001) 347-382 [hep-th/0105267].

[5] J. Ambjørn, J. Jurkiewicz and R. Loll: *Emergence of a 4D world from causal quantum gravity*, Phys. Rev. Lett. 93 (2004) 131301 [hep-th/0404156].

[6] J. Ambjørn, J. Jurkiewicz and R. Loll: *Reconstructing the universe*, preprint Utrecht, May 2005 [hep-th/0505154].

[7] J. Ambjørn, J. Jurkiewicz and R. Loll: *Semiclassical universe from first principles*, Phys. Lett. B 607 (2005) 205-213 [hep-th/0411152].

[8] J. Ambjørn, J. Jurkiewicz and R. Loll: *Spectral dimension of the universe*, preprint Utrecht, May 2005 [hep-th/0505113].

[9] R.M. Wald: *The thermodynamics of black holes*, Living Rev. Rel. 4 (2001) 6, http://www.livingreviews.org/lrr-2001-6 [gr-qc/9912119].

[10] S. Das: *Black hole thermodynamics: Entropy, information and beyond*, Pramana 63 (2004) 797-816 [hep-th/0403202].

[11] D.N. Page: *Hawking radiation and black hole thermodynamics* [hep-th/ 0409024].

[12] D. Kappel: *Nichtperturbative Pfadintegrale der Quantengravitation durch kausale dynamische Triangulierungen* (in German), Diploma Thesis, Univ. Potsdam (2001).

[13] P. Di Francesco and E. Guitter: *Critical and multicritical semi-random (1+d)-dimensional lattices and hard objects in d dimensions*, J. Phys. A 35 (2002) 897-928 [cond-mat/0104383].

[14] G. Viennot: *Heaps of pieces I: basic definitions and combinatorial lemmas*, in *Proc. Colloque de Combinatoire Énumérative*, eds. G. Labelle and P. Leroux, Lect. Notes in Math. 1234 (1986) 321-346.

[15] D. Benedetti, R. Loll and F. Zamponi, to appear.

[16] B. Dittrich and R. Loll: *A hexagon model for 3D Lorentzian quantum cosmology*, Phys. Rev. D 66 (2002) 084016 [hep-th/0204210].

[17] M. Bojowald: *Spherically symmetric quantum geometry: States and basic operators*, Class. Quant. Grav. 21 (2004) 3733-3753 [gr-qc/0407017].

[18] L. Brewin: *Marginally trapped surfaces in a simplicial space*, Phys. Rev. D 38 (1988) 3020-3022.

[19] B. Dittrich: *Dynamische Triangulierung von Schwarzloch-Geometrien* (in German), Diploma Thesis, Univ. Potsdam (2001).

[20] J. Ambjørn, J. Jurkiewicz, R. Loll and G. Vernizzi: *Lorentzian 3d gravity with wormholes via matrix models*, JHEP 0109 (2001) 022 [hep-th/0106082].

[21] J.W. York, Jr.: *Initial data for collisions of black holes and other gravitational miscellany*, in *Frontiers in numerical relativity*, eds. C.R. Evans, L.S. Finn and D.W. Hobill, Cambridge University Press, Cambridge, UK (1989) 89-109.

[22] R.M. Wald, *General relativity*, University of Chicago Press, Chicago (1984).

[23] M. Domagala and J. Lewandowski: *Black hole entropy from quantum geometry*, Class. Quant. Grav. 21 (2004) 5233-5244 [gr-qc/0407051].

[24] A. Ashtekar and B. Krishnan: *Isolated and dynamical horizons and their applications*, Living Rev. Rel. 7(2004) 10, http://www.livingreviews.org/lrr-2004-10 [gr-qc/0407042].

[25] J. Thornburg: *A fast apparent horizon finder for three-dimensional Cartesian grids in numerical relativity*, Class. Quant. Grav. 21 (2004) 743-766 [gr-qc/0306056].

[26] S.A. Hayward: *On the definition of averagely trapped surfaces*, Class. Quant. Grav. 10 (1993) L137-L140 [gr-qc/9304042].

[27] A.P. Gentle: *Regge calculus: a unique tool for numerical relativity*, Gen. Rel. Grav. 34 (2002) 1701-1718 [gr-qc/0408006];
R.M. Williams: *Recent progress in Regge calculus* Nucl. Phys. Proc. Suppl. 57 (1997) 73-81 [gr-qc/9702006].

[28] F. Kottler: *Über die physikalischen Grundlagen der Einsteinschen Gravitationstheorie*, Annalen der Physik 56 (1918) 401-462.

[29] P. Painlevé: *La Mécanique classique et la théorie de la relativité*, C. R. Acad. Sci. (Paris) 173 (1921) 677-680;
A. Gullstrand: *Allgemeine Lösung des statischen Einkörperproblems in der Einsteinschen Gravitationstheorie*, Arkiv. Mat. Astron. Fys. 16 (1922) 1-15.

[30] K. Martel and E. Poisson: *Regular coordinate systems for Schwarzschild and other spherical spacetimes*, Am. J. Phys. 69 (2001) 476-480 [gr-qc/0001069].

[31] R. Sorkin: *The electromagnetic field on a simplicial net*, J. Math. Phys. 16 (1975) 2432-2440 [Erratum-ibid. 19 (1978) 1800].